Development and characterization of a non-human primate model of central post-stroke pain

（非ヒト霊長類を用いた脳卒中後疼痛モデルの確立およびその評価）

平成 29 年度

長坂和明

筑波大学大学院　人間総合科学研究科　感性認知脳科学専攻

Table of contents

Chapter 1. General introduction

1-1. Introductory remarks

Stroke is a major cause of death and long-term disability worldwide, and these problems are being addressed by a wide variety of research fields, including pharmacology, medicine, and neuroscience (Strong *et al.*, 2007; Kim & Bae, 2017). Neuroscience research has provided important insights into the mechanisms underlying dysfunction associated with stroke and recovery by rehabilitation.

Artificial damage to the primary motor cortex (MI), the area essential for movement of the extremities, resulted in motor paralysis in animal models, characterized by difficulty in gripping and walking (Armstrong, 1988; Murata *et al.*, 2008; Murata *et al.*, 2015). However, the animals sometimes showed spontaneous recovery from motor paralysis. This was thought to be due to neural plasticity, with undamaged brain regions compensating for the lost function (Nudo *et al.*, 1996; Dimyan & Cohen, 2011; Murata *et al.*, 2015; Ishida *et al.*, 2016). Investigation of neural plasticity using various methods, including molecular biology, histology, electrophysiology, will help to elucidate the mechanisms underlying behavioral and cognitive changes after brain damage, and will also contribute to the development of novel clinical interventions such as drugs.

Neural plasticity, mentioned above, is an example of beneficial plastic changes that improve functional recovery. However, neural plasticity may also have negative effects on brain function (Vance *et al.*, 2009; Dietz, 2012). A research topic of current interest regarding negative effects of plasticity is neuropathic pain, which develops after nerve injury (Woolf & Salter, 2000; Bliss *et al.*, 2016). Central post-stroke pain (CPSP), which is addressed here, has also been suggested to be caused by central nervous system plasticity (Apkarian, 2011). Animal models using rodents have been developed and characterized to reveal the plasticity underlying CPSP (Wasserman & Koeberle, 2009; Hanada *et al.*, 2014). However, some brain structures and functions differ between rodents and primates (Kaas, 2004; Wallis, 2012). Therefore, CPSP models using animals with brain structures and functions closer to those of humans are important for elucidating the underlying mechanisms. Here, a new animal model of CPSP was established using rhesus macaques (Experiment 1), which are closer to humans in both the brain structure and function. Histological analyses were then performed to confirm glial activation, which is considered to be involved in the abnormal pain (Experiment 2). In addition, to investigate increased activity of brain regions associated with CPSP, whole-brain activity in the macaque model was measured in the pre- and post-lesion periods using functional magnetic resonance imaging (fMRI). The causal relationships between brain activities

and CPSP were then confirmed by pharmacological inactivation (Experiment 3).

1-2. Characteristics of CPSP

First, the clinical findings of CPSP are introduced in this section. The findings of clinical studies provide important insight into the underlying pathophysiological mechanisms.

1-2-1. Epidemiology

In addition to major symptoms such as early onset of hemiparesis, speech disabilities, and sensory deficits, late-onset pain also appears frequently as a result of cerebral vascular accidents (Leijon *et al.*, 1989; Bowsher, 1995; Kumar *et al.*, 2009). CPSP, a type of neuropathic pain, is a chronic pain syndrome associated with sensory abnormalities due to lesions in the somatosensory pathways of the central nervous system (Montes *et al.*, 2005; Kumar *et al.*, 2009; Krause *et al.*, 2012; Sprenger *et al.*, 2012). CPSP was reported to occur after lateral medullary infarction (Wallenberg syndrome), pontine stroke, lateral midbrain stroke, posterolateral thalamus stroke, secondary somatosensory cortex stroke, and insular cortex stroke (Hosomi *et al.*, 2015). CPSP is observed among in up to 10% of stroke patients (Hosomi *et al.*, 2015), and the prevalence rate is high among patients with lateral medullary stroke (25%) or thalamus lesions (25%) (Andersen *et al.*, 1995;

MacGowan *et al.*, 1997). Age, sex, stroke type (infarct or hemorrhage), and lesional hemisphere are not consistent predictors of CPSP (Klit *et al.*, 2009).

1-2-2. Pain characteristics

Typically, CPSP can emerge at any time from several weeks to several years after stroke (Kumar *et al.*, 2009; Hosomi *et al.*, 2015). Patients with CPSP complain about not only spontaneous pain but also evoked pain in which normally innocuous stimuli are perceived as painful, i.e., allodynia, or normally painful stimuli are perceived as even more painful, i.e., hyperalgesia. More than 90% of patients with CPSP show abnormalities in either thermal (cold or hot) or pain sensation (Leijon *et al.*, 1989; Andersen *et al.*, 1995). The abnormal pain is felt in the body region that is affected by sensory abnormalities, which corresponds topographically to the brain regions affected by the stroke lesion (Vestergaard *et al.*, 1995). Thus, the pain symptoms commonly occur in the range from half of the body to restricted body areas contralateral to the lesion (Klit *et al.*, 2009; Klit *et al.*, 2011; Hosomi *et al.*, 2015). In rare cases, some patients with CPSP have pain symptoms in areas of the body ipsilateral to the lesion (Kim, 1998). CPSP often reduces patients' quality of life and frequently interferes with rehabilitation (Kumar *et al.*, 2009).

1-3. Physiological pain pathways and CPSP

The mechanisms that produce allodynia or hyperalgesia resulting from brain lesions are poorly understood, as the basic mechanisms of physiological pain have not been fully elucidated. “Pain processing systems” are constructed by multiple ascending pathways and a wide range of brain areas that are involved in two major aspects of pain, i.e., perception and emotion. First, the anatomical pathways associated with pain, the pain matrix, are discussed (Chapter1, 1-3-1 and 1-3-2). Then, evidence is presented indicating that the same pathways are involved in the occurrence of CPSP.

1-3-1. Pathways from the spinal cord to the thalamus

Peripheral sensory neurons, which have thinly myelinated fibers (Aδ) and unmyelinated C fibers, are activated by noxious stimuli. Aδ fibers transmit intense mechanical sensation, and C fibers transmit noxious mechanical, thermal, and chemical sensation. Both of these fiber types terminate in laminae I, II, and deeper lamina V of the spinal dorsal horn. Anatomical tracer studies in non-human primates and rodents indicated that nociceptive information is conveyed across the midline within the spinal cord and is mainly transmitted to the ventral posterolateral nucleus (VPL), ventral posteromedial nucleus (VPM), ventral medial posterior nucleus (VMpo), and mediodorsal nucleus (MD) of the

thalamus through the lateral spinothalamic tract (Apkarian & Hodge, 1989; Apkarian & Shi, 1994; Almeida *et al.*, 2004; Craig, 2004; 2008; Dum *et al.*, 2009). The fibers also send branches to the lateral medulla, pons, or midbrain (Almeida *et al.*, 2004) (Fig. 1).

Sensory neurons with myelinated Aβ fibers principally transmit proprioceptive and cutaneous information, i.e., somatic sensation, from a dermatome. Generally, the Aβ fibers mainly terminate in the lamina V neurons, which then project to the ipsilateral brainstem through spinal dorsal columns. The information is then conveyed to the contralateral side of the medulla toward the thalamus, where the projections mainly terminate in the VPL and VPM (Francis *et al.*, 2008; McGlone & Reilly, 2010).

1-3-2. Pain-associated pathways from the thalamus to the cerebral cortex

The thalamus acts as a center of communication between many subcortical brain regions and the neocortices, and is divided into multiple subdivisions based on differences in architecture and both afferent and efferent connectivity. Here, the thalamic regions involved in pain are described.

The neurons in the VPL with noxious responses mainly project to the primary and secondary somatosensory cortices, whose pathways are called the lateral pain system, and are involved in processing sensory features, such as the duration and location of pain

(Kniffki & Mizumura, 1983; Kenshalo *et al.*, 1988; Andersson *et al.*, 1997; Greenspan *et al.*, 1999; Ploner *et al.*, 1999). On the other hand, the medial pain system, i.e., the pathway from the VMpo and MD to limbic structures, includes the cingulate and insular cortices (Saper, 1982; Hatanaka *et al.*, 2003; Brooks & Tracey, 2005; Dum *et al.*, 2009). As patients with lesions in these regions show altered emotional responses to pain (Foltz & White, 1962; Berthier *et al.*, 1988), the pathways are thought to mediate affective and motivational aspects of pain (Bushnell *et al.*, 2013).

1-3-3. Lesion sites and development of CPSP

From an anatomical perspective, CPSP is typically associated with stroke lesions at multiple sites in the lateral spinothalamic tract and its terminations, which are involved in noxious transmission (pain and temperature) (Hosomi *et al.*, 2015). Transmission of somatic sensory signals through the dorsal column pathway is typically spared in CPSP (Fig. 1). Importantly, it is still unclear whether the occurrence of CPSP is due to lesions of the MD or VMpo of the thalamus (Krause *et al.*, 2012; Hosomi *et al.*, 2015).

Krause et al. mapped the lesion areas using T1-weighted anatomical brain imaging in 18 patients presenting with CPSP of thalamic origin, and found critical lesions in the VPL of the thalamus in these patients (Krause *et al.*, 2012). The VPL, in which the

spinothalamic tracts are known to terminate, is therefore a key area for the occurrence of CPSP.

1-4. Figure and figure legend

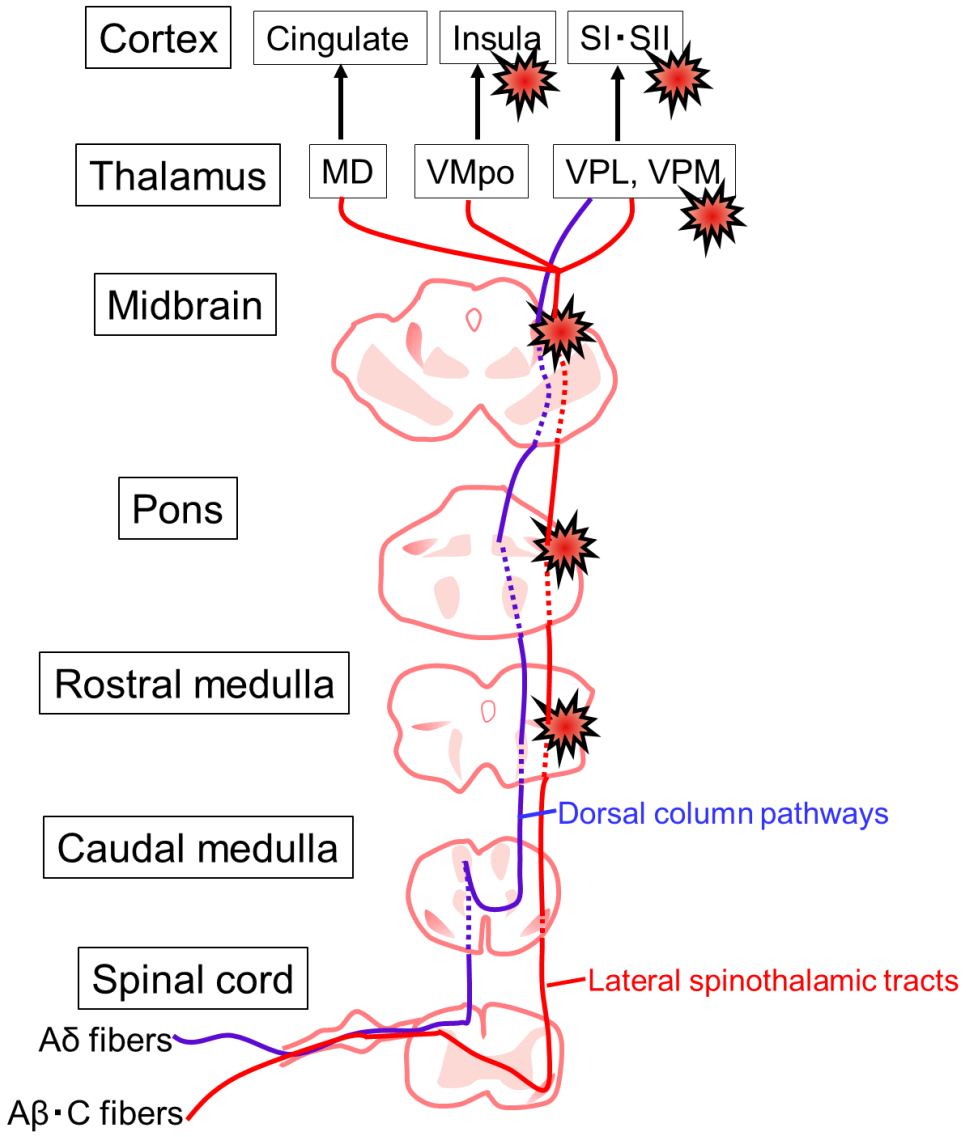

Figure 1. Stroke sites associated with occurrence of CPSP. A simplified illustration of spinothalamic and thalamocortical pathways is summarized from the anatomical investigations on the pathways. Cortico-cortical pathways are not shown. The lateral spinothalamic tracts (red line) carry information from the spinal dorsal horn to the thalamus through the caudal medulla, rostral medulla, pons and midbrain. CPSP occurs

in case somewhere in this pathway is lesioned. On the other hand, the dorsal column pathways (blue) are typically spared in CPSP patients. The figure is modified from Hosomi et al., 2015 and Brooks and Tracey, 2005.

Chapter 2. [Experiment 1] Behavioral changes after a focal lesion of the VPL

2-1. Introduction

2-1-1. Rodent models of CPSP

The CPSP is often caused by lesion of the lateral spinothalamic tract, however, its pathogenic mechanisms are not well understood. To address this problem, development of animal models for CPSP had been anticipated. In 2009, Wasserman and Koeberle first developed the CPSP animal model using rats based on hemorrhagic lesion in the VPL (Wasserman & Koeberle, 2009). Subsequently, many labs have investigated behavioral and histological changes in the rodent models following the induction of hemorrhage (Wasserman & Koeberle, 2009; Castel & Vachon, 2013; Hanada *et al.*, 2014; Kuan *et al.*, 2015; Shih *et al.*, 2017) or infarct (Takami *et al.*, 2011; Tamiya *et al.*, 2013; Blasi *et al.*, 2015) in the VPL. In clinical researches, pain perception is estimated by report from individual patients using the Visual Analogue Scale (subjective assessment of pain magnitude). However, in animal studies, the pain perception has to measure the behavioral response to presumed noxious stimulation (Percie du Sert & Rice, 2014). A lot of CPSP rodents model showed increased withdrawal responses to thermal and mechanical stimuli, which suggest the occurrence of characteristic symptoms of CPSP

patients (Wasserman & Koeberle, 2009; Takami *et al.*, 2011; Castel & Vachon, 2013; Tamiya *et al.*, 2013; Hanada *et al.*, 2014; Blasi *et al.*, 2015; Kuan *et al.*, 2015; Shih *et al.*, 2017), and several studies assessed efficacy of a drugs on the behavioral change (Hanada *et al.*, 2014; Kuan *et al.*, 2015).

2-1-2. Non-human primate model of CPSP

In addition to these CPSP models using rodents, the model using the macaque monkey can also contribute both to understanding CPSP mechanisms and to developing novel therapeutic interventions for CPSP because the macaque monkey is more compatible with human in regard to functions and structures of brain regions which is suggested to be involved in allodynia and hyperalgesia by brain imaging study of human patients as described below (Willoch *et al.*, 2004; Ducreux *et al.*, 2006; Casey *et al.*, 2012). Previous meta-analysis of fMRI and positron emission tomography (PET) experiments in patients with abnormal pain after peripheral nerve damage and brainstem stroke suggest that brain activity of the lateral and medial pain pathways were significantly increased, compared with normal pain in healthy human subjects (Lanz *et al.*, 2011). Moreover, a recent MRI study using voxel-based morphometry (VBM) indicates that the patients with CPSP are accompanied by a maladaptive atrophy in several cortical areas including the sensory and

prefrontal cortices, where sensory and emotional aspects of pain are processed (Krause *et al.*, 2016). These evidence strongly suggest that functional or structural plasticity occurs in a wide-range of brain regions, and therefore it is important to elucidate plasticity that underlies CPSP. However, some of the brain structures and functions are known to be different between rodents and primates (Kaas, 2004; Wallis, 2012).

2-1-3. Complex sensory systems of non-human primates

In the rhesus macaque, the primary somatosensory cortices, which are associated with sensory aspects of pain (Bushnell *et al.*, 1999), are clearly differentiated into four subdivisions, *i.e.,* Brodmann's areas 3a, 3b, 1 and 2 (Kaas, 2004). Areas 3b and 1 are known to receive projections from neurons in the contralateral spinal laminae I and V via the spinothalamic tract and VPL. Area 3b forms a systematic representation of the contralateral body surface, which contains both non-nociresponsive (response to touch) and nociresponsive (response to pain or temperature) neurons. Equally, area 1 is highly dependent on projections from area 3b for activation, and thus this area also contains a second systematic representation of tactile receptors of the contralateral body surface. Both area 3a, just rostral to area 3b, and area 2, just caudal to area 1, are activated by muscle spindle receptor activity from ventroposterior superior nucleus (VPS), which is

concerned with the proprioceptive sensation (Garraghty *et al.*, 1990). However, it has been suggested that the architecture (*i.e.,* Brodmann's areas 3a, 3b, 1 and 2) and functional divisions (*i.e.,* pain, touch, temperature and proprioception) in rodents are not clearly differentiated and are different from those of primates (Kaas, 2004).

2-1-4. Comparative anatomy of the monkey and rodent frontal cortex

Moreover, the macaque monkey shares homology with the human in respect to anatomical and physiological features of the prefrontal cortex, such as medial prefrontal, dorsolateral prefrontal and orbitofrontal areas, which are involved in the emotional aspects of pain (Treede *et al.*, 1999; Apkarian *et al.*, 2005). Comparative anatomy of rat, monkey and human frontal cortex are reviewed by Wallis (Wallis, 2012). Briefly, prefrontal cortex of human and monkey contains three architectonic subdivisions, agranular cortex, dysgranular cortex and granular cortex (Wallis, 2012). By contrast, several lines of studies have suggested that the rat frontal cortex only has agranular cortex (Ongur & Price, 2000; Wallis, 2012).

2-1-5. Hemorrhagic lesion in macaque VPL using collagenase type IV

In this thesis, hemorrhagic stroke was chosen because this cerebrovascular accident is

known to cause CPSP (Leijon *et al.*, 1989; Vestergaard *et al.*, 1995; Greenspan *et al.*, 2004), and the thalamus is one of the most common region of hemorrhagic stroke in humans (Fewel *et al.*, 2003).

The difference of the brain sizes as well as brain structures between the monkey and rodent is thought to be an important factor in development of animal models. In the developed rodent models, collagenase type IV, a protease which degrades blood vessels and induces hematoma and edema (Rosenberg *et al.*, 1990), was injected at the site of VPL with reference to the atlas which coordinates to induce a hemorrhage. Since the target site was small, the hemorrhagic lesion sometimes spread beyond the intended site (Blasi *et al.*, 2015). The macaque brain is larger than the rodent one, and therefore provides advantage of an experimental manipulation; making a focal lesion in VPL, which is essential for reproducing symptoms like human patients (Blasi *et al.*, 2015), is easier in the macaque than the rodents.

The VPL is known to have receptive fields on the upper body (Kaas *et al.*, 1984). It is reported that pain after a stroke is felt in the body part corresponding to the somatotopic representation of the affected brain region (Vestergaard *et al.*, 1995). In the present study, to make allodynia and hyperalgesia appear in the monkey's hand, I intended to induce a localized lesion to the receptive field on the hand within the VPL. I firstly confirmed the

location of VPL from the structural MRI of each individual brain, and then identified the subdivisions that respond to a somatic stimulation of the hand by using electrophysiological method (see Materials and Methods of Experiment-1 for detail). Thereafter, collagenase type IV was injected to the identified site of the VPL.

2-1-6. Assessment of allodynia and hyperalgesia in macaque monkey

I focused on the development of allodynia and hyperalgesia after a hemorrhagic lesion in macaque VPL because patients with CPSP frequently report the symptoms; non-painful mechanical or thermal stimuli (hot or cold) are perceived as painful after the lesion (Klit *et al.*, 2009). I considered that the development of allodynia and hyperalgesia can be measured objectively by estimating the changes of withdrawal responses to mechanical or thermal stimulation, i.e., the decrease of withdrawal threshold to the mechanical stimulation (in grams) and thermal stimulation (in sec) after the VPL lesion.

Because withdrawal responses of monkeys are the index to evaluate allodynia and hyperalgesia, the motor function should not be affected by hemorrhagic lesion. Thus, it is thought that the precise identification of location of VPL using electrophysiological techniques can prevent damage of the posterior capsule, which carries corticospinal tracts passing near the VPL.

2-2. Materials and Methods

2-2-1. Subjects

Four male adult rhesus macaques (*Macaca mulatta*) were used in the present study (Table 1). The macaques were purchased from a local provider (Hamri Co., Ltd., Ibaraki, Japan). The animal use protocol was approved by the Institutional Animal Care and Use Committee of the National Institute of Advanced Industrial Science and Technology (AIST), and were carried out in accordance with guidelines within the "Guide for the Care and Use of Laboratory Animals" (Eighth ed., National Research Council of the National Academies).

2-2-2. Identification of VPL and collagenase injection

An artificial stroke was induced unilaterally in the VPL—in the left hemisphere for Macaques I and P, and the right for Macaques C and S (Table 1). After a scalp incision was made, the skull was exposed, and two MRI-compatible head posts were attached to the skull under sterile conditions and pentobarbital anesthesia (25 mg/kg). The location of the VPL was determined for each animal, using stereotaxic coordinates from structural MRI of each macaque's brain obtained with a 3.0 T MRI system (Philips Ingenia 3.0 T,

Philips Healthcare, Best, the Netherlands). Before the scan, the macaques were anesthetized using medetomidine (0.05 mg/kg), midazolam (0.3 mg/kg), and ketamine (4 mg/kg), and then fixed in a magnet-free stereotaxic frame. The MRI protocols consisted of a T1-weighted turbo field echo sequence (repetition time (TR)/echo time (TE), 7.3/3.2 ms; number of excitations (NEX), 2; flip angle, 8°; field of view, 134 mm × 134 mm; matrix, 224 × 224; slice thickness, 0.6 mm; number of slices, 200) and a T2-weighted turbo spin echo sequence (TR/TE, 1500/283 ms; NEX, 2; flip angle, 90°; field of view, 134 mm × 134 mm; matrix, 224 × 224; slice thickness, 0.6 mm).

Following the MRI, the VPL sub-region involved in tactile sensation of the hand digits was identified by electrophysiological recordings. The microelectrode was penetrated at 1-mm intervals on the cortical surface, and the somatotopic organization of the VPL was determined by recording multiunit activity during light tactile stimuli applied to the contralateral body surface with a small hand-held brush. Collagenase type IV (C5138; Sigma, St. Louis, MO, USA; 200 U/ml in saline) was then injected in the identified VPL sub-region where neurons were activated by tactile stimuli (Fig. 2a-d). A single 4-μl injection of collagenase type IV was given to Macaque C, two 4-μl injections separated by 1 mm in the dorsoventral direction were given to Macaques P and I, and four 4-μl injections separated by 1 mm in both dorsoventral and rostrocaudal directions were

given to Macaque S (Table 1).

2-2-3. Behavioral procedures

To evaluate pain perception on the hands after the collagenase injection into the VPL, both mechanical and thermal withdrawal tests were performed. During the test, the macaque sat in a primate chair made of acrylic glass, and the wrists of both forelimbs were fixed to a horizontal plane positioned at the height of the macaque's waist. An opaque board was placed between the face and forelimbs; thus, the macaque did not see its own hand while mechanical or thermal stimuli were applied to it. A mechanical withdrawal test was conducted by using an electronic von Frey anesthesiometer (IITC Life Science, Inc., Woodland Hills, CA, USA) (Fig. 3a). Each von Frey filament was applied perpendicularly to the palmar surface of the second, third, and fourth fingers, and the maximum pressure exerted (in grams) that triggered hand withdrawal was assessed. Two trials were performed for each finger, and the larger pressure was adopted as the datum for that day. The withdrawal thresholds for both hands, one contralateral and the other ipsilateral to the affected VPL (*i.e.*, the contra-lesional and ipsi-lesional hands), were measured 4 days/week during weeks 1 to 4 and 2 days/week during weeks 5 to 12 after collagenase injection, and then compared to those obtained before lesion induction.

On the same day, a thermal withdrawal test was also conducted by using a thermal stimulator (SCP-85; As One Corporation, Osaka, Japan) (Fig. 3b). The plate surface was maintained at 55–45°C (for heat stimuli), 37°C (for control stimuli) or 10–5°C (for cold stimuli), and the macaque's hand was transferred to the plate. Although the macaque freely escaped from hot stimuli, to avoid the risk of low-temperature burn injury from prolonged contact with the plate, the duration of a single trial was designed to be no more than 1 min. Multiple trials (maximum, five) were performed at each temperature until the total contact time with the plate exceeded 90 s. To assess the degree to which the thermal stimulus affected withdrawal latencies, the latency for thermal stimulation was divided by that for control stimulation at 37°C. This ratio before lesion induction was compared to that after lesion induction for both hands. Hand withdrawal latencies were estimated in real time during the withdrawal test. In addition, the movements of both hands during the test were recorded, by using two digital video cameras (HC-V520M; Panasonic, Osaka, Japan) installed around the task apparatus, and a subset of the video data was re-analyzed by a person blinded to the treatment of the macaques. The results of this re-analysis were consistent with those of the real-time assessments.

2-2-4. Confirmation of lesion site

To evaluate the spatiotemporal changes of a stroke, structural MRI scans were performed before, and 1 day, 4 days, 1 week, 2 weeks, 1 month, and 3 months after collagenase injection. The MRI protocols with both T1- and T2-weighted sequences were the same as those described above. The areas that contained edema and hematoma were seen as a region of high and low signal intensities, i.e. hyperintense and hypointense areas, in T2-weighted MRI, respectively (Mack *et al.*, 2003; Kleinschnitz *et al.*, 2005; West *et al.*, 2009; Zhao *et al.*, 2014). The unbiased volumes for both edema and hematoma were calculated by Cavalieri's principle (Mayhew, 1992), using StereoInvestigator imaging software (MBF Bioscience, Williston, VT, USA). In the atlas-based analysis, the T2-weighted MRIs of macaques that received a collagenase injection into the right hemisphere was flipped along the mid-sagittal plane, so that the stroke area was located on the left side of the brain. These processed MRIs were matched to macaque brain template (voxel size, 0.5 × 0.5 × 0.5 mm) (Black *et al.*, 2004) by using SPM12 software (http://www.fil.ion.ucl.ac.uk/spm/). After individual images were processed as described, the areas with hypointense signals were delineated manually as regions of interest and overlaid onto the template by using MRIcro software (http://www.mricro.com). The size and location of the lesion induced by collagenase injection were also evaluated by histological analysis. Briefly, the macaques were deeply anesthetized with sodium

pentobarbital (35–50 mg/kg, *i.v.*) and then perfused through the ascending aorta with 0.5 L of ice-cold saline containing 2 mL (2000 units) of heparin sodium followed by ice-cold fixative containing 4% paraformaldehyde and 0.1% glutaraldehyde. The brains were then immediately removed and blocked in the coronal plane (5 mm thick). The blocks were immersed in a post-fixative solution containing 2% paraformaldehyde and 5% sucrose in phosphate buffer for several hours, followed by successive immersions in sucrose solutions. They were embedded in optical cutting temperature compound (Miles Inc., Elkhart, IN, USA), and rapidly frozen in a dry ice-acetone bath. Brain segments were sectioned coronally at a thickness of 18 μm on a cryostat (a Shandon Cryotome SME; Thermo Electron Corporation, Pittsburg, PA, USA) and then Nissl-stained with cresyl fast violet (Higo *et al.*, 2002; 2004; Higo *et al.*, 2010). Images of the Nissl-stained sections were photographed under an Olympus BX60 microscope by using a 3CCD color video camera (DV-47d; MBF Bioscience) and then digitized using StereoInvestigator imaging software. The lesioned area was defined as the area of a dense concentration of small cells (5–10 μm in diameter), which presumably includes both glial cells and blood cells, and unbiased volumes were calculated using the same method as that for structural MRI analysis.

2-2-5. Statistical analysis

All data are presented as medians and interquartile ranges. Statistical significance was assessed by nonparametric tests including a two-tailed Mann–Whitney U-test, Wilcoxon signed-rank test, and Kruskal–Wallis one-way analysis of variance (ANOVA) with Dunn's *post hoc* test. Statistical results were considered significant at $P < 0.05$. The statistical analyses were performed using GraphPad Prism software (GraphPad Software Inc., San Diego, CA, USA).

2-3. Results

2-3-1. Stroke and lesion sizes

A T2-weighted MRI of a rhesus macaque (Macaque I) 1 day after collagenase injection shows that the stroke area, which was seen as a hypointense core and a surrounding hyperintense rim, was mainly localized around the thalamus (arrow in Fig. 4a). The areas of both hypointense and hyperintense signal intensity expanded from day 1 to day 3 after the injection; this may result from expansion of the hematoma and edema (Fig. 4b, c). These areas then decreased rapidly over the course of 2 weeks, when the hyperintense area almost disappeared. Thereafter, the residual hypointense area was almost stable until the end of the experiment 3 months after injection (Fig. 4b). T2-weighted MRIs of the

other three macaques (Macaques C, P and S) also indicated a stroke mainly localized around the thalamus, and the volume dynamics were similar to that in Macaque I (Fig. 4d, e). A normalized MRI brain template with atlas-based borders indicated that the stroke area at 3 days after collagenase injection, when the stroke was largest, included several other thalamic nuclei in addition to VPL (Fig. 4f). By contrast, the stroke area was mainly localized within VPL ≥2 weeks after injection. The collagenase-induced lesion was also histologically estimated by using Nissl-stained coronal sections (Fig. 5). We defined the lesioned area as the area of a dense concentration of small cells (5–10 μm in diameter) (Fig. 5a), which presumably include both glial cells and blood cells (Mracsko & Veltkamp, 2014). The serial coronal sections of Macaque I indicated that the lesion was located within the VPL of the thalamus (arrows in Fig. 5c–e). The histological lesion was also localized within the VPL of Macaque C. In Macaque S, however, lesions were observed not only in the VPL but also in adjacent thalamic nuclei, *i.e.,* the caudal part of the ventral lateral nucleus (32% of the total lesion volume) and the reticular nucleus (4%), as well as in other brain areas including the caudate nucleus (17 %, Table 1).

2-3-2. Behavioral changes after collagenase injection

To determine whether a VPL lesion alters pain perception, I evaluated withdrawal

responses to both mechanical and thermal stimuli applied to the surface of the hands of the macaques before and after collagenase injection. Before the injection, the withdrawal responses to both mechanical and thermal stimuli were almost identical for both hands (Fig. 6a, b). Moreover, the median withdrawal latencies for thermal stimulation at 50°C did not significantly differ from those for control stimulation (37°C) ($P = 0.8646$, Mann–Whitney U-test, for the hand contralateral to the hemisphere to be subjected to collagenase injection), and the ratios of the withdrawal latency for thermal stimulation to that for control stimulation before injection were close to 1 for both hands (Fig. 6b), indicating that the macaques consistently responded to each stimulus. During the first 2–3 days after collagenase injection, all four macaques showed mild paralysis of the hind-limb contralateral to the injected hemisphere. This may be due to the fact that the posterior internal capsule where pyramidal tracts control hind-limb movements was temporarily affected by stroke because it is located adjacent to the VPL (Schmahmann & Pandya, 2006). There was no apparent impairment of movements for other body parts, such as the forelimb and face, and the macaques showed no difficulty in grasping a piece of food or in eating and drinking. Moreover, the withdrawal responses to both mechanical and thermal stimuli during the first week after injection were almost identical to those before injection (Fig. 6a, b), indicating that the macaques' hand movements during the

withdrawal tests were not affected by the stroke. The lack of motor paralysis in the forelimb indicates that stroke spared the portion of the posterior internal capsule where pyramidal tracts control forelimb movements; this site is located several millimeters rostral to VPL (Schmahmann & Pandya, 2006).

A Kruskal–Wallis test revealed significant changes in both the withdrawal threshold for mechanical stimulation and the ratio of the withdrawal latency for thermal stimulation to that for control stimulations on the hand contralateral to the injected hemisphere (*i.e.,* contra-lesional hand) across weeks after the injection (Fig. 6a, b, $P < 0.0001$, respectively). Dunn's *post hoc* analyses demonstrated a statistically significant reduction in both the withdrawal threshold for mechanical stimulation (Fig. 6a, $P < 0.0001$) at 8 weeks and the ratio of the withdrawal latency for thermal stimulation to that for control stimulation (Fig. 6b, $P = 0.0051$) at 4 weeks after injection compared with those before injection, respectively. The behavioral changes were interpreted as indicating the occurrence of both mechanical allodynia and thermal hyperalgesia. The reductions lasted until the end of the behavioral experiments, 3 months after the injection. There was no correlation between the degree of the reduction and the dosage of collagenase, *e.g.*, the ratios of the withdrawal threshold at 12 weeks after the injection to that before injection were 0.68, 0.27, 0.51, and 0.55 in Macaques C (4μl), I (8μl), P (8μl), and S

(16μl), respectively. I did not observe significant change for mechanical withdrawal responses on the hand ipsilateral to the injected hemisphere, *i.e.*, the ipsi-lesional hand (Fig. 6a). Although the median ratio of the withdrawal latency on the ipsi-lesional hand for thermal stimulation at 50°C to that for control stimulation showed a tendency to decrease, the decrease was not statistically significant (Fig. 6b). Even though no motor paralysis was detected after collagenase injection, all four macaques rarely used the contra-lesional hand to retrieve food in their cages; this behavior suggests that mechanical allodynia developed in the contra-lesional hand. I also evaluated changes in withdrawal latency for thermal stimulation at temperatures other than 50°C (Fig. 6c). No significant change was observed for withdrawal latency on either the contra- or ipsi-lesional hands for thermal stimulation at 45°C or cold stimuli (10–5°C) at 3 months after the injection. The withdrawal latency for thermal stimulation at 55°C compared with that for control stimulation before injection was less than 1 for both hands, indicating that the intact monkeys sensed thermal stimulation at 55°C as a nociceptive stimulus. I measured withdrawal latency to thermal stimulation at 55°C to confirm that the macaques remained able to withdraw in response to nociceptive stimuli after collagenase injection. The withdrawal latency to stimulation at 55°C did not increase after collagenase injection, suggesting a lack of motor impairment. Rather, it significantly decreased for both hands

at 3 months after the injection compared with the value before injection ($P < 0.0001$, Mann–Whitney U-test), although the latency on the ipsi-lesional hand was longer than that on the contra-lesional hand at 3 months after injection ($P = 0.0464$, Wilcoxon signed-rank test). These results suggest that mild hypersensitivity to heat stimuli occurred in the ipsi-lesional hand.

2-4. Discussion

In Experiment-1, I developed a primate model of CPSP based on a hemorrhagic focal lesion induced in the VPL of rhesus macaques. The lesioned macaques showed behavioral changes that were interpreted as the development of both allodynia to mechanical stimulation and hyperalgesia to hot thermal stimulation.

In rodent models of CPSP, the onsets of mechanical allodynia and thermal hyperalgesia occur within 1 week after hemorrhage induction by injecting collagenase around the VPL (Wasserman & Koeberle, 2009; Castel *et al.*, 2013; Hanada *et al.*, 2014). However, a majority of patients with CPSP begin to complain of the abnormal pain a delay of several weeks after a stroke (Kumar *et al.*, 2009). A similar delay in the onset of CPSP was recently reported in rats based on focal ischemic lesion in thalamus by injection of endothelin-1 (Blasi *et al.*, 2015). Unfortunately, this model exhibited thermal

hyperalgesia but not mechanical allodynia, which is one of the most common symptoms of patients with CPSP (Bowsher, 2005; Klit *et al.*, 2009). Thus, the present model using macaques, in which significant behavioral changes to both mechanical and thermal stimuli were observed after 4 weeks when edema and hematoma was stabilized from the induction of hemorrhage, more faithfully reproduced the symptoms of CPSP patients than the other experimental animal models. The difference between the present and previous models may reflect a species difference or differences in the size and location of the lesion. In recent models using rodents, the injection sites for collagenase type IV and endothelin-1 were determined using stereotaxic coordinates. In the experiment, in contrast, the injection site was determined not only by structural MRI of an individual macaque but also by the result from electrophysiological recordings in which the location of the VPL sub-region responsive to tactile stimulation of the hand digits was identified. These techniques, in combination with the relatively large brain of rhesus macaques, contributed to inducing a hemorrhagic lesion within the VPL more focal than those induced in previous rodent models.

Although I observed behavioral changes in the contra-lesional hand that were interpreted as reflecting development of both mechanical allodynia and thermal hyperalgesia, behavioral changes interpreted as the development of mild thermal

hyperalgesia were also ascertained in the ipsi-lesional hands. Kim (1998) reported that some human patients with severe CPSP have milder sensory symptoms on the side ipsilateral to the lesion than the side contralateral to the lesion. It has been reported that there are certain indirect sensory pathways, the spino-reticulo-thalamic pathways involved in distributing pain and arousal terminate in bilaterally medial thalamus (Carstens *et al.*, 1990; Kim, 1998; Villanueva *et al.*, 1998). Moreover, a recent study reported bilateral cortical atrophy in patients with CPSP (Krause *et al.*, 2016). The physiological and pathophysiological anatomical findings suggest that unilateral thalamus lesion may contribute to the bilateral sensation of abnormal pain. The present macaque model will aid in understanding plastic changes in neuronal structures involved in the bilateral symptom.

The present macaque models did not display behavioral changes reflective of hyperalgesia to cold stimulation which are also common in the patients with CPSP. However, I do not consider that the lack of cold hyperalgesia in the present macaque model indicates a critical difference from symptoms of human patients because reduction or less of cold sensation was reported in human patients in case the lesion is confined to the ventral posterior area in the thalamus (Kim *et al.*, 2007).

Note that the stroke area at 3 days after injection of collagenase, when the stroke

area was largest, included several other thalamic nuclei, such as the pulvinar and MD nuclei. Therefore, plastic changes resulted from damage to thalamic nuclei other than the VPL may continue even after the stroke has stabilized and might participate to induce CPSP. The present study is the first to use MRI to demonstrate the spatiotemporal changes of a thalamic stroke and suggests that lesions based on histological confirmation after the completion of behavioral tests may be substantially underestimated because stroke lesion size transiently increased and finally decreased after stroke.

In the case of using this new macaque model, a next important step may be to investigate how the size and location of the lesion affect the symptoms of CPSP.

2-5. Figures and figure legends

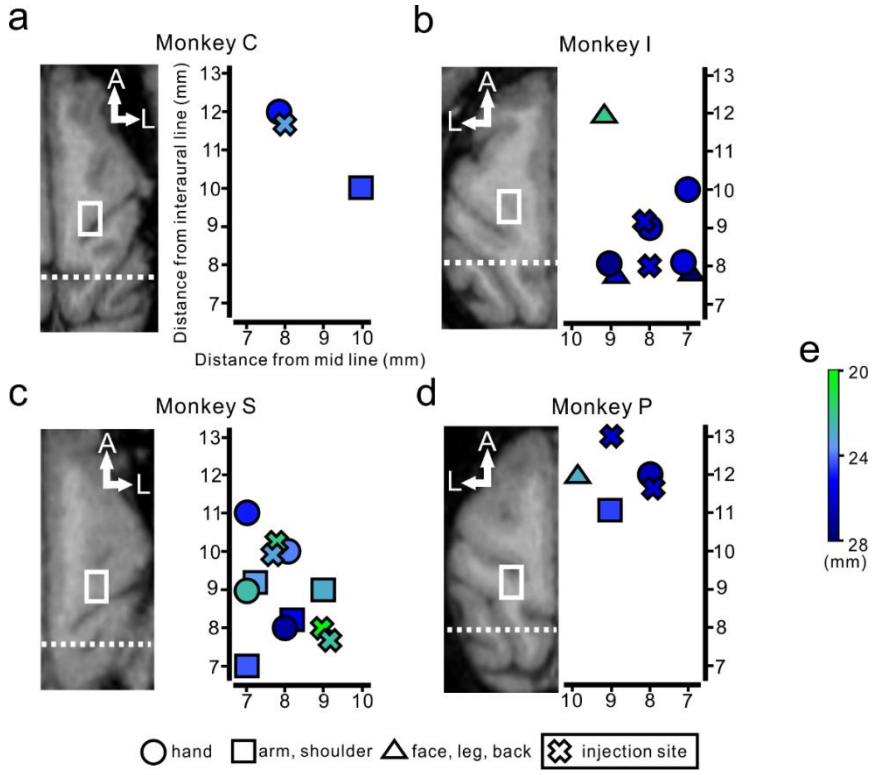

Figure 2. Electrophysiological identification of hand area in VPL. (**a-d**) Coordinate representation of sensory response and the site of collagenase injection (cross). The symbols (circle, quadrate and triangle) indicate representative somatotopic organization derived using multiunit activity recording during tactile stimulation applied to the contralateral body parts. The white rectangle and dotted line on the axial MR image including VPL (depth is 5 mm from the cortical surface) of each macaque indicate the recording area and interaural line, respectively. The depth profiles of all symbols from cortical surface (in mm) were represented as a color related to scale bar (**e**). A, Anterior; L, Lateral.

a

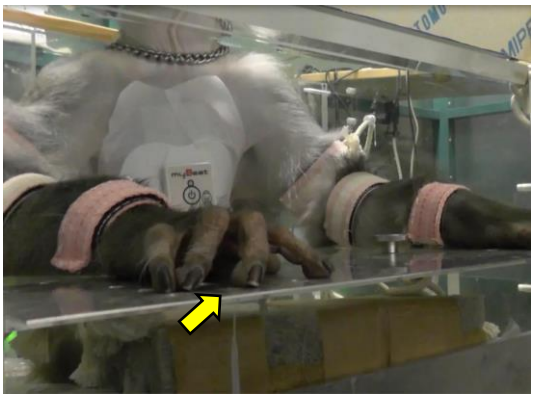

b

Figure 3. Assessment of withdrawal response. During behavioral tests, the monkey sat in the primate chair and experience the mechanical withdrawal test using von Frey filaments (**a**) and thermal withdrawal test using thermal stimulator (**b**). Yellow arrow in (**a**) shows contact point between the von Frey filament and dorsal surface of the digit.

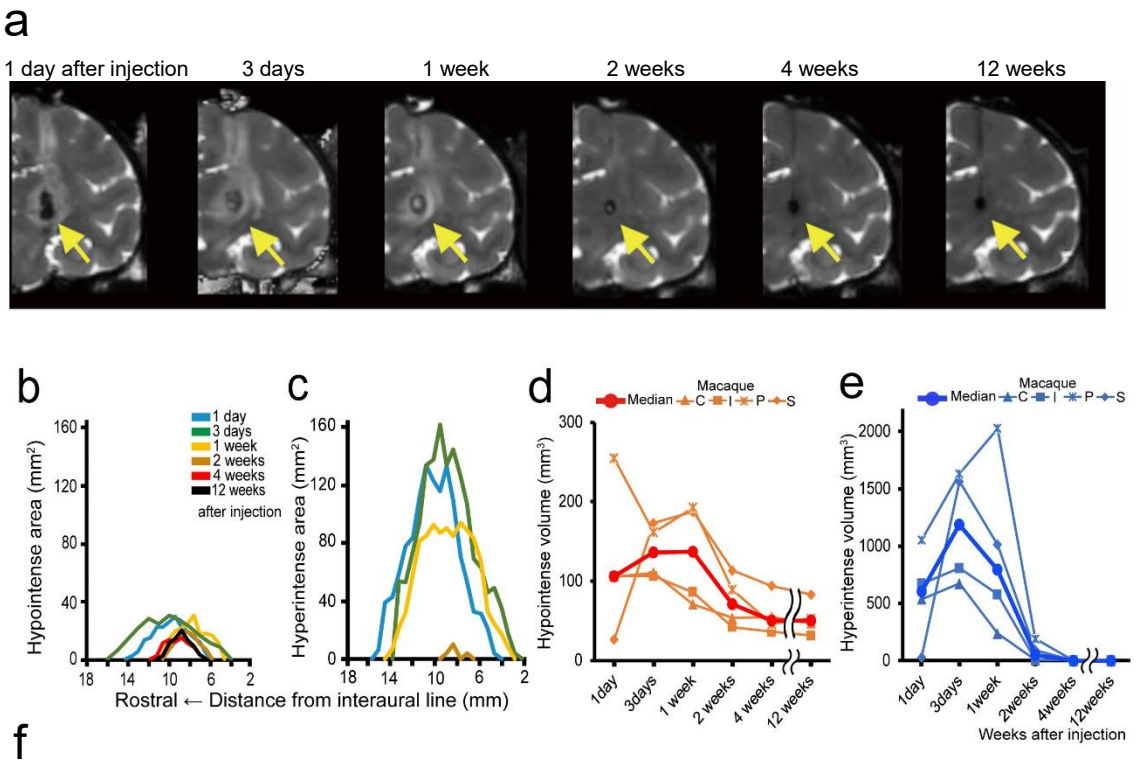
a
1 day after injection
3 days
1 week
2 weeks
4 weeks
12 weeks
b
Hypointense area (mm²)
1 day
3 days
1 week
2 weeks
4 weeks
12 weeks
after injection
Rostral ← Distance from interaural line (mm)
c
Hyperintense area (mm²)
d
Macaque
Median C I P S
Hypointense volume (mm³)
1day
3days
1 week
2 weeks
4 weeks
12 weeks
e
Macaque
Median C I P S
Hyperintense volume (mm³)
Weeks after injection
f
3 days after lesion
2 weeks
12 weeks
Cd
LD
VLc
VLo
VLps
LP
MD
VPL
VPM
VPI
CM
Pul
SG
GLd
R
+12mm
+10mm
+8mm
+6mm
+4mm
Number of subjects
1 2 3 4

Figure 4. Time course of stroke after injection. (**a**) Coronal T2-weighted MRIs of Macaque I showing time course of stroke after the injection. The area that contained a hematoma and edema was seen as the hypointense stroke core (arrows) and the surrounding hyperintense rim. The coronal images were obtained through the rostro-caudal level at which the VPL is located. (**b**, **c**) Temporal changes of the hypointense (**b**) and hyperintense areas (**c**) in successive coronal images of Macaque I are shown as a function of rostral distance from the interaural line. In this macaque, 4 to 17 mm rostral to the interaural line corresponds to the level at which the thalamus is located. (**d**, **e**) Temporal volume changes of the hypointense (**d**) and hyperintense areas (**e**) are shown for all four collagenase-injected rhesus macaques. In all animals, the areas of both hypointense and hyperintense signal intensity decreased at 2 weeks after the collagenase injection, when the hyperintense area almost disappeared. Thereafter, the residual hypointense area was almost stable until 12 weeks after injection. (**f**) Using a normalized MRI brain template and atlas-based borders, it was indicated that the stroke area at 3 days after collagenase injection included the VPL and several additional thalamic nuclei. However, at 2 weeks and 12 weeks after injection and thereafter, the lesion was mainly localized within VPL. The colors indicate the number of macaques with hypointense signals in the indicated voxels. Cd, caudate nucleus; CM, central medial nucleus; GLd,

dorsal lateral geniculate nucleus; LD, lateral dorsal nucleus; LP, lateral posterior nucleus; MD, mediodorsal nucleus; Pul, pulvinar nucleus; R, reticular nucleus; SG, suprageniculate nucleus; VLo, oral part of the ventrolateral nucleus; VLc, caudal part of the ventrolateral nucleus; VLps, ventrolateral nucleus, pars postrema; VPM, ventral posteromedial nucleus; VPI, ventral posteroinferior nucleus; VPL, ventral posterolateral nucleus.

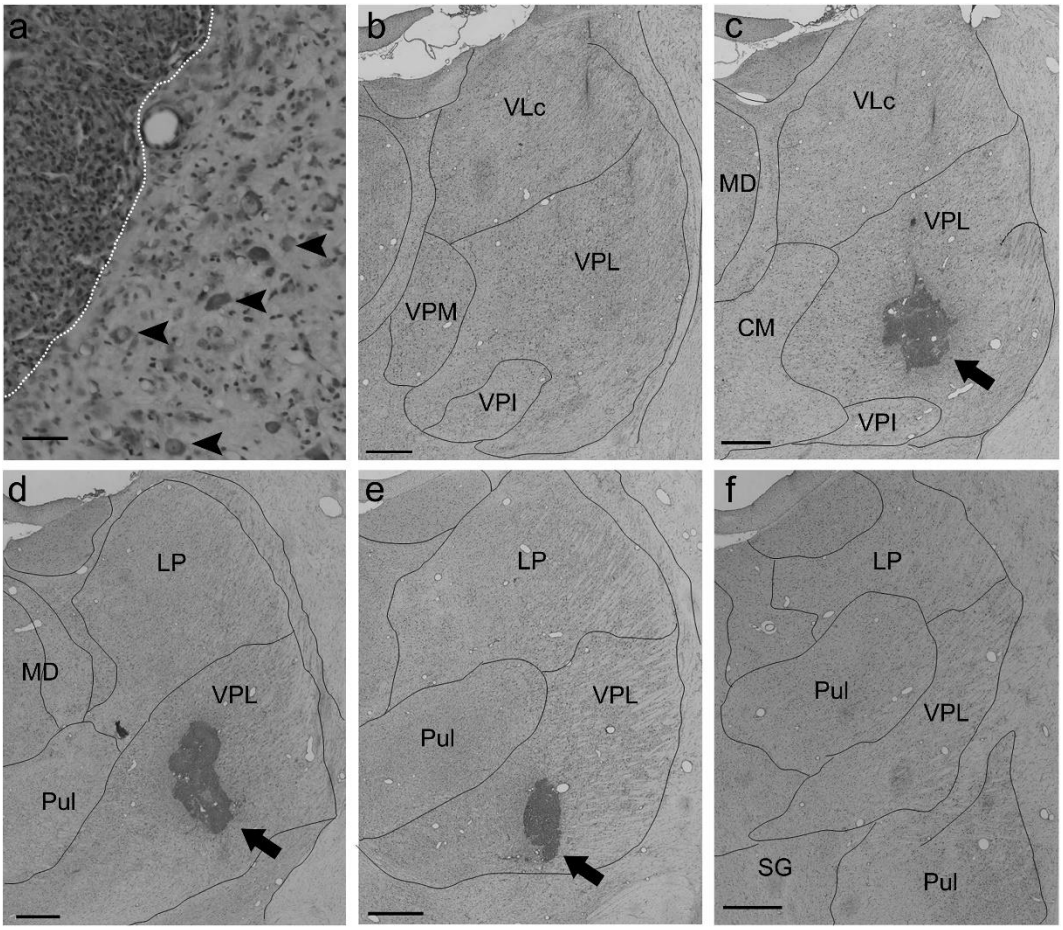

Figure 5. Confirmation of lesional area. (**a**) A Nissl-stained coronal section showing both the lesional and perilesional areas in the VPL. The lesional area was defined by a dense concentration of small cells (5–10 μm in diameter), which presumably includes both glial cells and blood cells. The boundary between the lesional and perilesional areas is indicated by the white dotted line (left, lesional area; right, perilesional area). Large cells (20–40 μm in diameter, arrowheads) presumed to be neurons were observed in the perilesional area. Scale bar: 50 μm. (**b-f**) Serial Nissl-stained coronal sections of Macaque

I, spaced by approximately 600 μm, are arranged from rostral (**b**) to caudal (**f**). Note that the lesion was located within the VPL. Scale bar: mm. CM, central medial nucleus; LP, lateral posterior nucleus; MD, mediodorsal nucleus; Pul, pulvinar nucleus; SG, supragenicular nucleus; VLc, caudal part of the ventrolateral nucleus; VPM, ventral posteromedial nucleus; VPL, ventral posterolateral nucleus; VPI, ventral posteroinferior nucleus.

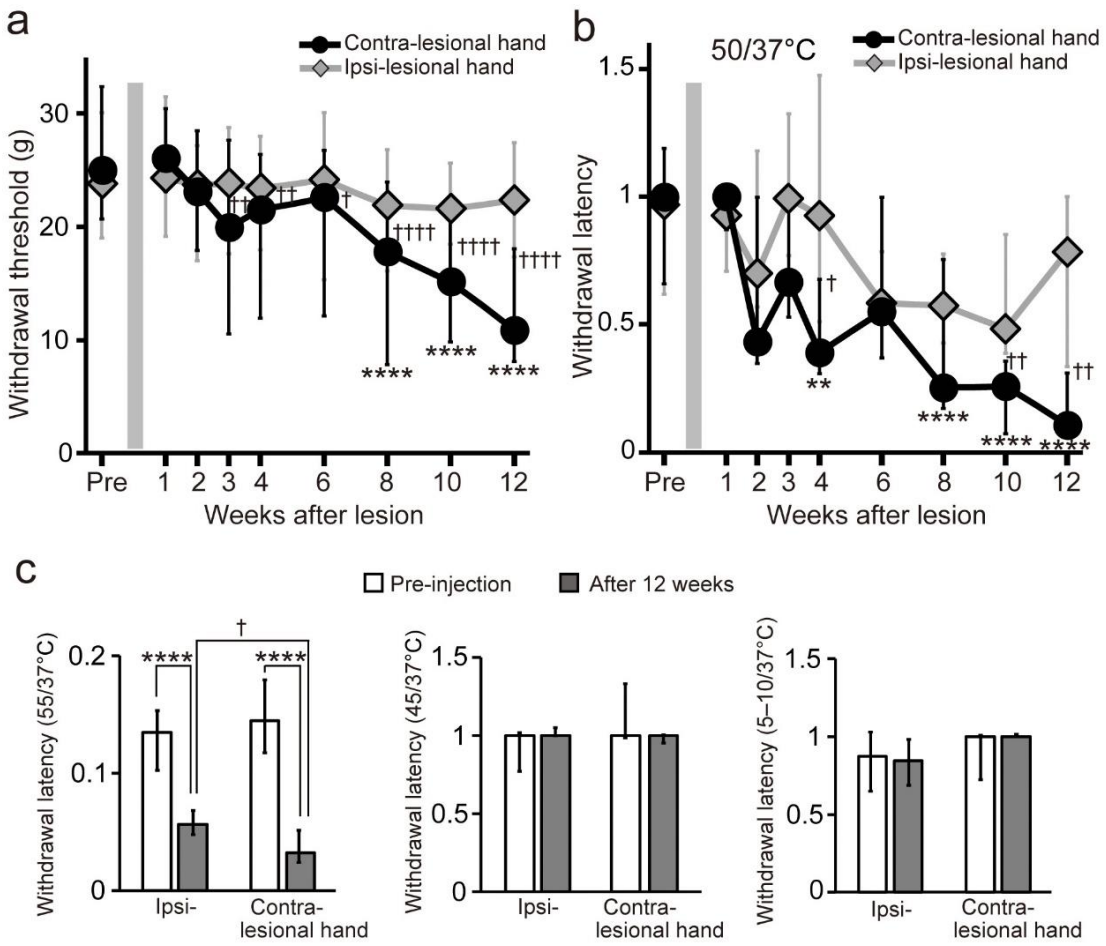

Figure 6. Behavioral changes after collagenase injection. (**a**, **b**) Weekly changes in the withdrawal response to mechanical and thermal stimulation. The withdrawal thresholds, shown as the pressure exerted (in grams, **a**), and the latencies, represented as the ratio of the withdrawal latency for thermal stimulation (50°C) to that for control stimulation (37°C, **b**), are shown for both hands, one contralateral (contra-lesional hand) and the other ipsilateral (ipsi-lesional hand) to the injected hemisphere. Medians and interquartile ranges for the four collagenase-injected macaques are shown. Several weeks following

the injection, both the withdrawal threshold for mechanical stimulation and withdrawal latency for thermal stimulation on the contralateral hand significantly decreased relative to those before the injection, but not observed on the ipsilateral hand. The reductions lasted until the end of the behavioral experiment 3 months after the injection. $^{**}P < 0.01$ and $^{****}P < 0.0001$, compared with pre-injection (Kruskal–Wallis one-way ANOVA followed by Dunn's *post hoc* test). $^{\dagger}P < 0.05$, $^{\dagger\dagger}P < 0.01$, and $^{\dagger\dagger\dagger\dagger}P < 0.0001$, compared with ipsi-lesional hand (Wilcoxon signed-rank test). (**c**) Medians and interquartile ranges for the withdrawal latency for thermal stimulations other than 50°C before and at 12 weeks after injection. The withdrawal latencies for 55°C on the both contra- and ipsi-lesional hands significantly decreased relative to those before injection ($^{****}P < 0.0001$, Mann-Whitney U test), although the latency on the ipsi-lesional hand was longer than that on the contra-lesional hand at 12 weeks after injection ($^{\dagger}P < 0.05$, Wilcoxon signed-rank test).

2-6. Table

Table 1. Collagenase-injected rhesus macaques used in the present study

	Weight, kg	Injected hemisphere	Dosage of collagenase, μl	Lesion volume, mm^3	Post-injection survival period, days
Macaque C	8.5	Right	4	2.1	104
Macaque I	8.0	Left	8	3.9	92
Macaque P	8.9	Left	8	−*	−
Macaque S	8.6	Right	16	7.3 (1.5) **	113

*Data not available because the macaque is not killed for this study.

**The lesion volume outside the thalamus is shown in parentheses.

Chapter 3. [Experiment 2] Evaluation of activated glial cells around lesion area

3-1. Introduction

3-1-1. Glial activation and neuropathic pain

Glial cells have recently attracted attention for their role in plasticity (Eroglu & Barres, 2010). Specifically, researchers in the field of neuropathic pain have been devoting considerable attention to glial cells because they are involved in pain symptoms and are therefore key to developing pain-relieving drugs. The relationship between glial cells and neuropathic pain after spinal cord and peripheral nerve injuries has been well studied in animals. In the first part of this section, I will briefly describe why glial cells are considered to be associated with abnormal pain.

Glial cells are classified into microglia, astrocytes, and oligodendrocytes. Microglia, which are the resident immune cells of the central nervous system, are dormant under normal conditions, but are immediately activated in response to several conditions, including systemic inflammation and brain injury (Ladeby *et al.*, 2005; Raivich, 2005). A previous report suggested that activated microglia in the dorsal horn may underlie the abnormal pain experienced following peripheral nerve and spinal cord injuries (Tsuda *et*

al., 2003). A well-known mechanism by which activated microglia induce pain is a "depolarizing shift of E_{GABA}" (γ-aminobutyric acid (GABA)-induced chloride ion response) (Tsuda, 2016), which is thought to result according to the following: (1) Activation of microglial P_2X_4 receptors (subtypes of an ionotropic receptor P_2X, of which there are seven types: P_2X_1–P_2X_7) stimulates the synthesis and release of brain-derived neurotrophic factor (BDNF) (Ulmann *et al.*, 2008). (2) Thereafter, BDNF alters several molecular pathways of spinal lamina I neurons and downregulates the neuronal chloride ion transporter (K-Cl cotransporter; KCC2) (Morgado *et al.*, 2011), which extrudes chloride ions from the cell (Hubner *et al.*, 2001). (3) As a consequence, GABA elicits excitatory depolarization, rather than inhibitory hyperpolarization, in the dorsal horn neurons with a decrease in KCC2 expression. Thus, when activated by nociceptive stimulation, the lamina I neurons produce aberrant nociceptive output to the thalamus and contribute to allodynia or hyperalgesia after nerve injury (Tsuda, 2016).

Astrocytes are also activated following nerve injury (Miyoshi *et al.*, 2008; Doyen *et al.*, 2017), and the activated astrocytes in the dorsal horn also contribute to abnormal pain. Miyoshi et al. (2008) found that interleukin (IL)-18 and IL-18 receptors were upregulated in activated astrocytes in the spinal dorsal horn after nerve injury, and functional inhibition of IL-18 signaling pathways attenuated the tactile allodynia.

3-1-2. Activated glial cells and CPSP

It has been recently reported that glial cells are also associated with allodynia or hyperalgesia following VPL lesion. Hanada et al. (2017) reported activated microglia in the vicinity of lesioned VPLs and reported that pain-like behaviors in a mouse model decreased following the infusion of minocycline, which is known to attenuate microglial activation (Bastos *et al.*, 2012). Additionally, successful reduction of pain was achieved by infusion of an antagonist of the P_2X_7 receptor (Kuan *et al.*, 2015), which is important for activating microglia in brain tissues (Monif *et al.*, 2010). These results led to the hypothesis that the interaction between the microglia and neurons in the VPL is also involved in the onset of CPSP. Hence, as the first step, I investigated histological changes in microglia and astrocytes and examined neuronal degeneration in the perilesional area using a macaque CPSP model.

3-2. Materials and methods

3-2-1. Subjects

Three male adult rhesus macaques (*Macaca mulatta*) were used in this study (Macaques C, I, and S; Table 1). I also used the brain tissues of three intact macaques weighing 5.1,

7.5, and 8.0 kg as the controls for the immunohistochemical analysis (see below). The macaques were purchased from a local supplier (Hamri Co., Ltd., Ibaraki, Japan). The animal use protocol was approved by the Institutional Animal Care and Use Committee of AIST, and the experiment was carried out in accordance with the Guide for the Care and Use of Laboratory Animals (Eighth edition; National Research Council of the National Academies).

3-2-2. Immunohistochemistry

The macaque tissues used for this experiment were prepared in the same manner as in Experiment 1.

To characterize the degree of microglial and astrocyte reactivity, and the extent of neuronal degeneration, I performed immunohistochemistry 3 months after the collagenase injection to detect the presence of ionized calcium-binding adaptor molecule 1 (Iba-1), glial fibrillary acidic protein (GFAP), and neuronal nuclear antigen (NeuN) on the brain sections obtained from Macaques C, I, and S. The immunohistochemistry analysis for each antigen was performed with a rabbit anti-Iba-1 polyclonal antibody (1:16,000, cat. no. 019-19741; Wako Pure Chemicals, Osaka, Japan), a rabbit anti-GFAP polyclonal antibody (1:125, cat. no. Z0334; Dako, Glostrup, Denmark), and a mouse anti-

NeuN monoclonal antibody (1:50, cat. no. MAB377; Chemicon, Temecula, CA, USA), respectively. The immunocomplex was visualized by the avidin-biotin-peroxidase method. The Vectastatin® Elite ABC Rabbit IgG Kit (PK-6101; Vector Laboratories, Inc., Burlingame, CA, USA) was used for Iba-1 and GFAP staining and the Vectastatin® Elite ABC Mouse IgG Kit (PK-6102; Vector Laboratories, Inc.) was used for NeuN staining. The color reaction was developed using diaminobenzidine for the substrate (Dojindo Laboratories, Kumamoto, Japan) according to the manufacturer's instructions. To investigate whether microglia and astrocytes were located in the vicinity of neurons in the perilesional VPL, double-labeling immunofluorescence was also performed. In the double-labeling experiments, either the anti-Iba-1 or the anti-GFAP antibody was incubated with the anti-NeuN antibody; it was then visualized using Alexa 488-conjugated goat anti-rabbit IgG and Alexa 546-conjugated goat anti-mouse IgG (Invitrogen, Waltham, MA, USA). Sections were washed and then covered with Fluoromount/Plus™ (Diagnostic Biosystems, Pleasanton, CA, USA).

To quantify the immunoreactivity in the perilesional area, the relative optical density (OD) for each antigen was measured in a 100-μm × 100-μm square that was randomly drawn around the border of the lesion using Image J software (National Institutes of Health, Bethesda, MD, USA). The OD was also measured in 200-μm × 200-

μm squares sampled at distances 100–300, 300–500, 500–700, 700–900, 900–1,100, and 1,100–1,300 μm from the border. For each antigen, 10 squares were measured for each distance, and the OD of the background staining was also measured in 10 200-μm × 200-μm squares that represented the neighboring white matter in each section. I evaluated the staining intensity by calculating the percentage of OD above the background level of each square in the perilesional VPL. Then, the OD value in the perilesional VPL was normalized to the average of the values obtained from the VPL of the contra-lesional hemisphere and the corresponding VPL of normal intact macaques.

3-2-3. Statistical analysis

All immunohistochemical data are presented as medians and interquartile ranges. Statistical significance was assessed by nonparametric tests, including a two-tailed Mann–Whitney U test and a Kruskal–Wallis one-way analysis of variance (ANOVA) with Dunn's *post hoc* test. Statistical significance was set at $P < 0.05$, and the analyses were performed using GraphPad Prism software (GraphPad Software Inc., San Diego, CA, USA).

3-3. Results

To characterize the degree of microglial and astrocyte reactivity, as well as the extent of neuronal degeneration, I performed immunohistochemistry 3 months after collagenase injection to detect Iba-1, GFAP, and NeuN on brain sections obtained from Macaques C, I, and S. Furthermore, I observed cells with shapes characteristic of activated microglia, *i.e.*, enlarged cells with thickened proximal processes and reduced ramification of distal branches (arrows in Fig. 7a) (Ladeby *et al.*, 2005; Raivich, 2005). Iba-1-positive cells were abundant not only in the lesional area, defined by a dense concentration of small cells (5–10 μm in diameter) in the Nissl-stained section, but also in the perilesional area, several hundred μm from the border of the lesional area (Fig. 7e). GFAP-positive cells were also abundant in the perilesional area at 3 months after collagenase injection (Fig. 7c, f). Additionally, I observed cells with shapes characteristic of activated astrocytes, *i.e.*, enlarged cell bodies and thick processes (arrows in Fig. 7c) (Sofroniew, 2009). No activated microglia or astrocytes were detected in the VPL of the hemisphere contralateral to the collagenase injection (Fig. 7b, d), and the OD values of the Iba-1 and GFAP of the VPL of the contra-lesional hemisphere did not significantly differ from those of normal intact macaques (Iba-1, $P = 0.5718$, GFAP, $P = 0.7412$, Mann–Whitney U test). I also performed immunohistochemistry for NeuN and confirmed the presence of neurons in the perilesional area, although the neurons close to the lesional area were less dense than

those in the intact VPL (Fig. 7g). Double-labeling immunofluorescence indicated that both Iba-1-positive microglia and GFAP-positive astrocytes existed in the vicinity of surviving neurons in the perilesional area, and the neurons were surrounded by the processes of the activated microglia and astrocytes (Fig. 8a, b).

3-4. Discussion

As described in the Introduction section in this chapter, previous studies using rodent models have shown that microglial activation is associated with the pathophysiology of CPSP (Wasserman & Koeberle, 2009; Hanada *et al.*, 2014; Kuan *et al.*, 2015), and that pain-like behaviors are reduced by infusions of minocycline and P_2X_7 receptor antagonists (Hanada *et al.*, 2014; Kuan *et al.*, 2015), which are known to attenuate microglial activation (Monif *et al.*, 2010; Bastos *et al.*, 2012). The present experiments also showed microglial activation both the perilesional and lesional areas. In contrast to the rodent CPSP models described above (Wasserman & Koeberle, 2009; Hanada *et al.*, 2014), in which significantly increased immunoreactivity in the perilesional area for Iba-1 was confirmed until 1 month post-injection, the present results showed a significant increase even at 3 months post-collagenase injection. Taken together with the results of a immunohistological study of rhesus macaques with a motor cortex lesion, which

demonstrated that microglial activation persists for 12 months after the lesion (Nagamoto-Combs *et al.*, 2007), the present results suggest that the temporal dynamics of microglial activation differ between primates and rodents. Thus, the macaque model of CPSP may have an advantage over the other experimental models for testing therapeutic interventions that last for several months, such as rehabilitative training and continuous pharmacological treatment.

Although there is no direct evidence to prove that abnormal excitation of neurons attributable to microglial activation occurs in CPSP patients, a previous study reported an unusual pattern of neural activity, *i.e.*, a burst discharge, in the perilesional area of patients with CPSP of thalamic origin (Hirato *et al.*, 2010). In a rodent model of CPSP, increased neural activity of the MD and the cingulate cortex were attenuated by suppressing microglial activation of the thalamus (Kuan *et al.*, 2015). This evidence indicates that plastic changes of neurons may occur not only in the perilesional area, but also in areas distant from the lesioned site.

3-5. Figures and figure legends

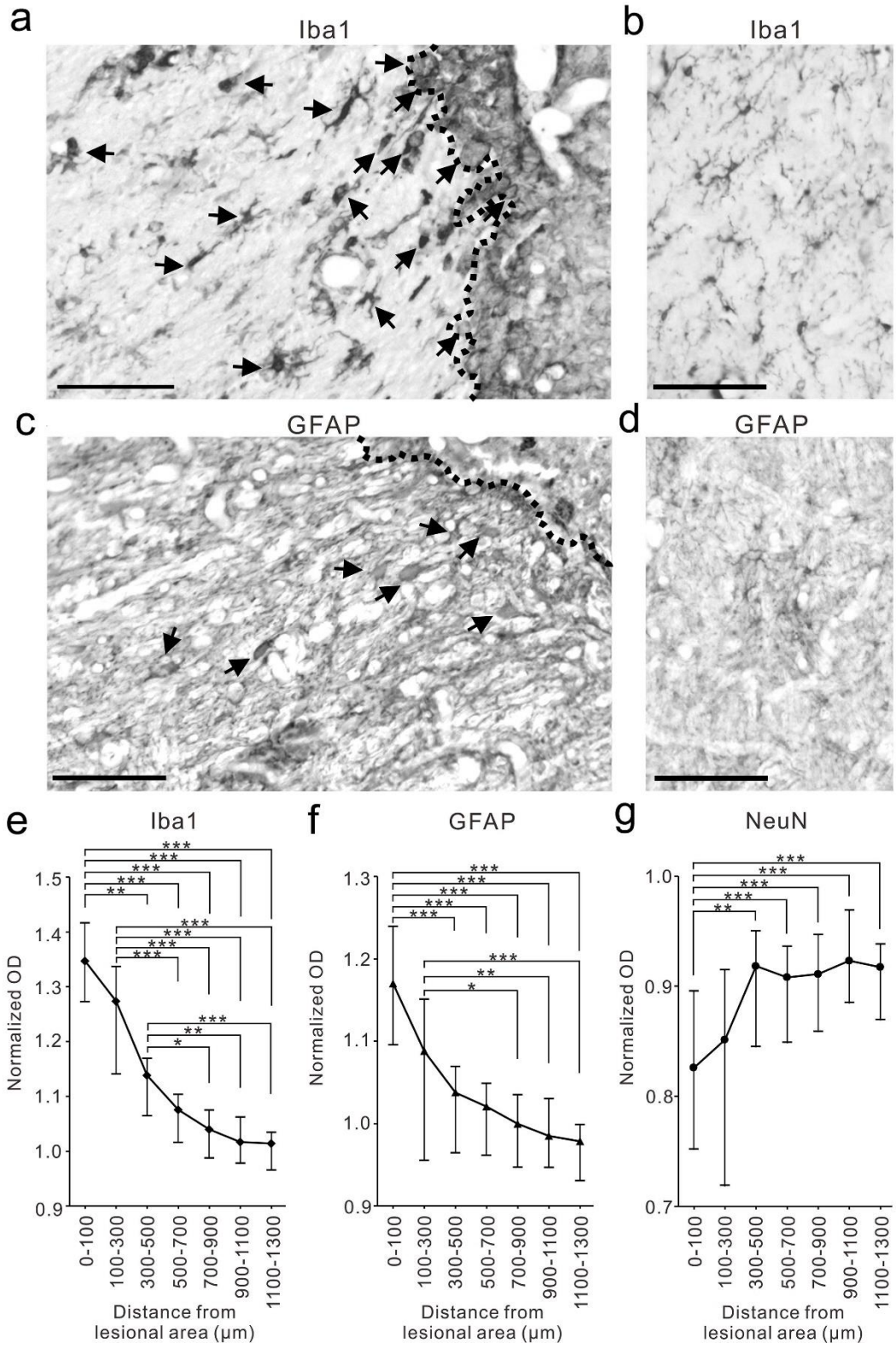

Figure 7. Glial activation in the perilesional area at 3 months after collagenase injection. (**a**-**d**) Coronal sections showing localization of the ionized calcium-binding adaptor molecule 1 (Iba-1) and glial fibrillary acidic protein (GFAP) in the VPL of both the collagenase-injected (**a**, **c**) and contralateral hemispheres (**b**, **d**). (**a**) Iba-1-positive cells were shown to have the characteristic shapes of activated microglia (*i.e.,* enlarged cells with thickening of proximal processes and reduced ramification of distal branches (arrows)) in the perilesional area (the left side of the dotted line). (**b**) No activated microglia were detected in the VPL of the contralateral hemisphere. (**c**, **d**) GFAP-positive cells with characteristic shapes of activated astrocytes (*i.e.,* enlarged cells with thickening of proximal processes) were observed in the perilesional area (arrows in **c**) but not in the contralateral hemisphere (**d**). Scale bar: 100 μm. (**e–g**) Immunoreactivities of Iba-1 (**e**), GFAP (**f**), and neuronal nuclear antigen (NeuN) immunoreactivity (**g**) in the perilesional area are shown as a function of distance from the border of the lesional area. The optical density (OD) of immunoreactivity was normalized to the values obtained from the VPL of the contra-lesional hemisphere and those in the corresponding VPL of normal intact macaques. $^{*}P < 0.05$, $^{**}P < 0.01$, and $^{***}P < 0.001$ (Kruskal–Wallis one-way ANOVA followed by Dunn's *post hoc* test).

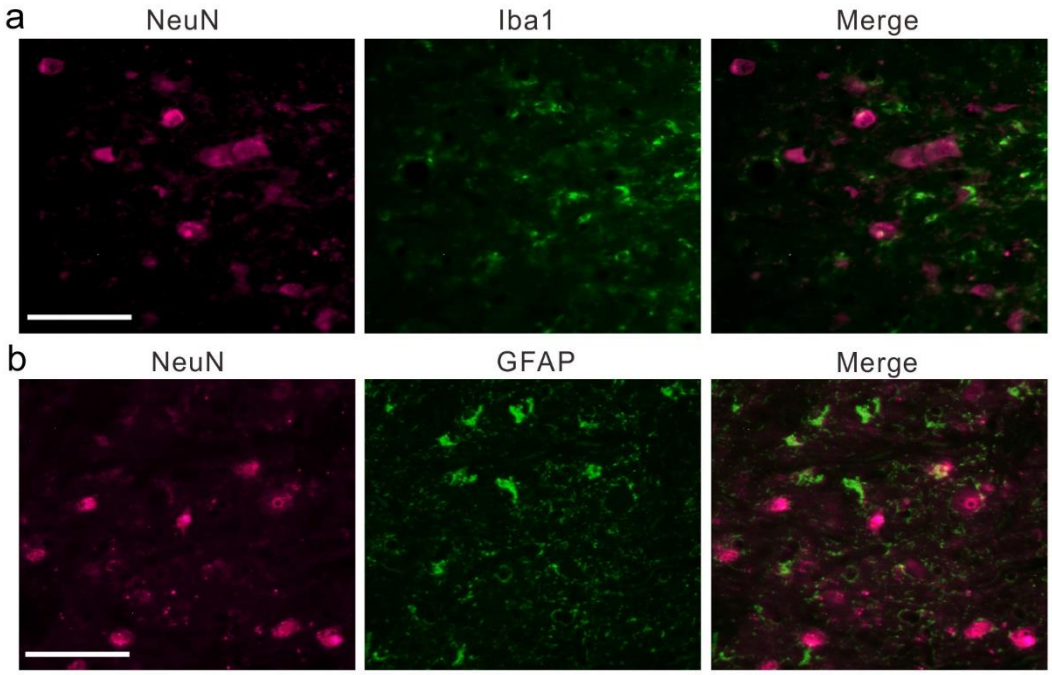

Figure 8. Surviving neurons in the perilesional area of the VPL were surrounded by processes of activated microglia and astrocytes. (**a**, **b**) Representative immunofluorescence images showing localizations of neurons (NeuN; magenta), microglia (Iba1; green in **a**), and astrocytes (GFAP; green in **b**) at < 200 μm from the border of the lesional area. Scale bar: 100 μm.

Chapter 4. [Experiment 3] Brain activity changes

4-1. Introduction

As described in Chapter 3, the interaction between chronically activated microglia and the surrounding neurons may influence neural activity not only in the vicinity of the lesioned VPL, but also in a wide range of other brain areas. Additionally, patients often experience allodynia and hyperalgesia long after a stroke, suggesting that the pathophysiology of CPSP is not an acute phenomenon, but rather a progressive condition associated with the neural plasticity of the pain processing area.

Whole-brain imaging techniques, such as positron emission tomography (PET) and functional magnetic resonance imaging (fMRI), are non-invasive and have been used to investigate the brain activities underlying pain perception (Talbot *et al.*, 1991; Moisset & Bouhassira, 2007). Studies using these techniques have found that activation in response to physiological pain consistently occurs in six brain regions: the thalamus, the primary somatosensory cortex (SI), the secondary somatosensory cortex (SII), the insular cortex (IC), the anterior cingulate cortex (ACC), and the prefrontal cortex (PFC) (Talbot *et al.*, 1991; Treede *et al.*, 1999; Apkarian *et al.*, 2005). Activation of these areas increases or extends when subjects experienced allodynia or hyperalgesia, whereas this was not the

case in healthy subjects with normal pain perception (Moisset & Bouhassira, 2007; Seifert & Maihofner, 2009; Lanz *et al.*, 2011). Additionally, it has been reported that the abnormal activities described above are diminished by administration of an analgesic drug (Iannetti *et al.*, 2005). However, it is difficult to determine the causal link between increased brain activity and abnormal pain because it is technically difficult to inactivate the brain areas involved in humans.

The homology of the pain-processing areas of rhesus macaques and humans (details in 2-1-3 and 2-1-4), and the relatively large brains of experimental animals, render the imaging data obtained in rhesus macaques comparable to those obtained in clinical research. Furthermore, the causal relationship can be confirmed by combining an invasive technique, in which brain activity is pharmacologically inactivated, with imaging data obtained from the macaque model of CPSP. However, a major problem arises with *in vivo* imaging of macaques: sedation is required to reduce the noise caused by bodily movements, but this may affect pain-related brain activity. To avoid this problem, I used propofol, which has little, if any analgesic, effect (Grounds *et al.*, 1987; Steinbacher, 2001) and followed the procedure employed in my previous study (Nagasaka *et al.*, 2017).

I hypothesized that the VPL lesion would cause abnormal pain (allodynia and hyperalgesia) through increased (or extended) brain activity around the lesioned area

and/or the pain-associated areas, and that pharmacological inactivation by microinjection of muscimol, a GABA receptor agonist, would decrease the abnormal pain if the brain activity was causally involved in the abnormal pain.

4-2. Materials and methods

4-2-1. FMRI

To investigate the changes in brain activity associated with mechanical allodynia and thermal hyperalgesia, fMRI scanning was performed in Macaque P using the 3.0 T MRI system (Ingenia 3.0 T; Philips, Amsterdam, The Netherlands) (Fig. 9a). Functional scan sequences consisted of field-echo, echo-planar imaging (EPI) (TR/TE, 3,000/35 ms; flip angle, 90°; field of view, 120 mm × 120 mm; matrix, 64 × 64; slice thickness, 2.0 mm; number of slices, 27). The fMRI scans were acquired using a block-design paradigm and were conducted before (pre-lesion) and at least 3 months after the collagenase injection (post-lesion), when both mechanical allodynia and thermal hyperalgesia were indicated by behavioral analyses. A mechanical stimulus paradigm was used in the fMRI scans to measure brain activity during mechanical stimulation; specifically, a somatosensory stimulus was applied to either the right (contra-lesional) or left (ipsi-lesional) hand by a small, hand-held MR-compatible brush. A single block consisted of two conditions, each

of which was preceded by a 30-sec no-stimulus period (Fig. 9b). Eighty blocks were performed before lesion induction, and 140 blocks were performed after the onset of CPSP. The fMRI scanning was also performed under the three thermal stimulus conditions of a thermal stimulus paradigm. Each of the following conditions was also preceded by a 30-sec no-stimulus condition (Fig. 9c): (1) 37°C control stimulation of both the right and left hand (R_{37}/L_{37}); (2) 50°C thermal stimulation of the right hand and 37°C control stimulation of the left hand (R_{50}/L_{37}); and (3) 50°C thermal stimulation of the left hand and 37°C control stimulation of the right hand (R_{37}/L_{50}). Thermal stimuli were applied to the hand by warm gel packs (Hakugen-Earth, Tokyo, Japan), which were conditioned at 50°C and 37°C in constant temperature chambers until just before scan onset. Forty blocks were performed before lesion induction, and 140 blocks were performed after the onset of CPSP. During scanning, the macaque was sedated by continuous intravenous infusion of propofol (0.4 mg/kg/min). The fMRI data were analyzed with SPM12 software (Wellcome Department of Cognitive Neurology, London, UK). Images were realigned and resliced according to the mean EPI to correct for head motion. They were then co-registered to the corresponding T1-weighted anatomical image and normalized to a macaque brain template (Rohlfing *et al.*, 2012). I confirmed that distortion in the brain structure induced by the collagenase injection was negligible.

The resulting image was smoothed with a 4 mm × 4 mm × 4 mm full-width at half-maximum Gaussian kernel. Voxel-wise statistical analysis was based on the generalized linear model. The contrasts were defined as “right hand stimulation − left hand stimulation” before and after lesion induction, respectively, to confirm regions in which the signal increased with mechanical allodynia. In terms of thermal stimulation, I defined the contrasts as “$R_{50}/L_{37} - R_{37}/L_{37}$ before injection” and “$R_{50}/L_{37} - R_{37}/L_{37}$ after injection”. A region in which thermal stimulation-related signals increased in the post-lesion period was examined by analyzing the contrasts. In experiments involving mechanical stimulation, the peaks were considered significant at a voxel threshold of $Z > 4.8$ ($P < 0.01$, corrected for multiple comparisons, one-tailed) and a cluster extent of five voxels. The peaks were considered significant at a voxel threshold of $Z > 2.3$ ($P < 0.01$, uncorrected for multiple comparisons, one-tailed) and a cluster extent of two voxels in experiments that used thermal stimulation. Statistical differences between the results of experiments using mechanical and thermal stimuli were considered when determining the block number. The statistical evaluation of the fMRI data in the present study was similar to those of previous fMRI and PET studies (Murata *et al.*, 2015; Nagasaka *et al.*, 2017).

4-2-2. Pharmacological inactivation

After 7 months following VPL lesion, brain microinjection of muscimol, a $GABA_A$ receptor agonist, was performed on the macaque which is performed fMRI experiments. In preparation for the injection, a plastic chamber was fixed to the skull under general anesthesia (see Materials and methods in Experiment-1 for details). The chamber was positioned over both the ACC and IC/SII. For the IC/SII, the chamber axis was positioned at an angle of 30° laterally from the vertical axis to prevent the needle from penetrating into the primary motor cortex.

Muscimol (5 μg/μL dissolved in 0.1 M phosphate buffer at pH 7.4; Sigma, St. Louis, MO, USA) was slowly injected with pressure at a rate of 1μL per min via a microsyringe (MS-10; Ito Corporation, Fuji, Japan) while the subject was under medetomidine anesthesia (0.05 mg/kg). Specifically, 3 μL of muscimol was injected at two sites of the ACC that were separated by 5 mm in a rostrocaudal direction (Fig. 12a, b), and at two sites of the IC/SII (Fig. 13a) that were separated by 5 mm in a depth direction. The tip of the injection needle was located just lateral to the ACC and medial to the IC/SII, and the orifice of the injection needle was oriented medially and laterally to allow the injected muscimol to diffuse toward the ACC (Fig. 12a, b) and IC/SII (Fig. 13a), respectively. The sites of muscimol injections were within the area where significantly increased brain activity had been observed in the fMRI experiment (Figs. 10c, 11c; Tables

2, 3). After injection, the needle was retained for 20 min to allow the solution to disperse, and to minimize backflow through the needle track. Thirty minutes after administration of atipamezole (0.125 mg/kg), an antagonist of medetomidine, the behavioral assessment described in the Materials and methods of Experiment-1 was conducted. The degree of inactivation of brain activity was evaluated by comparing the thresholds of the withdrawal responses to the mechanical and the thermal stimulation after injection of muscimol and vehicle (0.1 M phosphate buffer at pH 7.4). Four injections of both muscimol and vehicle were administered in each brain area.

4-2-3. Statistical analysis

All behavioral data are presented as medians and interquartile ranges. Statistical significance was assessed by nonparametric tests, including a two-tailed Mann–Whitney U test (GraphPad Prizm 6; GraphPad Software Inc., San Diego, CA, USA); differences were considered significant at $P < 0.05$.

4-3. Results

4-3-1. Changes of brain activation

The results of Experiment-1 reflected behavioral changes in the macaque used in the

fMRI experiment. At least 3 months after the VPL lesion, the right hand (contra-lesional hand) withdrawal threshold in response to the mechanical stimulation, and the withdrawal latency in response to the thermal stimulation (50°C), were significantly decreased compared with those before the lesion ($P < 0.001$, Mann–Whitney U test) (Fig. 10a, 11a), indicating both mechanical allodynia and thermal hyperalgesia.

To investigate changes in the response to the mechanical and thermal stimuli, fMRI scanning was performed under propofol sedation during the pre- and post-lesion periods. Before the lesion, activity associated with mechanical stimulation of the right hand was observed in several brain areas, including the SI and IC of the left hemisphere and the ventromedial prefrontal cortex (vmPFC) and caudate nucleus (Cd) of both hemispheres (Fig. 10b, Table 1); brain activity associated with thermal stimulation delivered to the hand was observed primarily in the Cd of both hemispheres (Fig. 11b, Table 2). The clusters showing activation were consistent with those identified in previous studies, indicating that somatosensory stimulation during anesthesia activates the sensory cortices as well as the Cd (Antognini *et al.*, 1997; Liu *et al.*, 2013).

During the post-lesion period, the mechanical stimulus-related activity indicated that mechanical stimulation of the right hand (contra-lesional hand) increased activity in a cluster located in the ACC, IC, and SII of the ipsi-lesional hemisphere (Fig. 10c, Table 2),

which are the brain regions known to show increased activity in patients with mechanical allodynia (Lanz *et al.*, 2011). Similarly, thermal stimulation of the right hand during the post-lesion period was associated with increased activity in a cluster located in the ACC, IC, and SII (Fig. 11c, Table 3), areas that have shown increased activity in patients with thermal hyperalgesia (Lanz *et al.*, 2011).

4-3-2. Effect of inactivation

If a causal relationship existed between increased activity in certain brain areas and allodynia or hyperalgesia, inactivation of these areas would result in a reduction of pain-like behaviors (*i.e.,* the withdrawal response to mechanical and thermal stimulation). Thus, the ACC and IC/SII were inactivated by a focal microinjection of muscimol. Although I did not directly confirm the spread of 3 μL muscimol, this dose has been shown to inactivate a spherical volume of macaque brain tissue roughly 5–6 mm in diameter (Murata *et al.*, 2015). Following inactivation of the ACC, both the withdrawal threshold to the mechanical stimulation and the withdrawal latency to the thermal stimulation (50°C) showed significant increases compared with those after vehicle injection (Fig. 12c, d). Similarly, when the IC/SII was inactivated, the withdrawal threshold and latency were significantly increased compared with the comparable values after vehicle injection (Fig.

13b, c). The withdrawal threshold in response to the mechanical stimulation returned to the level observed pre-lesion after the inactivation of both areas. By contrast, after inactivation, the withdrawal latency in response to the thermal stimulation remained lower than that before the lesion (inactivation of ACC, $P < 0.0001$; inactivation of IC, $P = 0.003$; Mann–Whitney U test).

4-4. Discussion

Overall, the current experiment demonstrated significant increases in brain activity associated with CPSP in the ACC, IC, and SII of the hemisphere ipsilateral to the lesion. Also, when these areas were inactivated by muscimol microinjection, the withdrawal responses to both the mechanical and thermal stimulation decreased. The present results suggest that neural activities in the ACC and IC/SII are crucial for both mechanical allodynia and thermal hyperalgesia after VPL lesion.

4-4-1. Measurement of brain activity in macaque under anesthesia

FMRI is important for studying the functional changes in the brain underlying CPSP because multiple brain regions are associated with pain processing (Talbot *et al.*, 1991; Moisset & Bouhassira, 2007). In this experiment, the monkey was sedated by continuous

intravenous infusion of propofol during fMRI scanning to prevent motion artifacts. A previous fMRI experiment done in rats under propofol sedation showed that the increase in blood oxygenation level-dependent (BOLD) signal intensity during somatosensory stimuli was dampened, but not completely suppressed, compared with that observed during consciousness (Lahti *et al.*, 1999). Another fMRI experiment in rats also detected reliable intensity changes in the somatosensory cortex during median nerve stimulation under propofol sedation (Scanley *et al.*, 1997; Lahti *et al.*, 1999). Moreover, it is known that propofol sedation has minimal effect on somatosensory evoked potentials in humans (Langeron *et al.*, 1999; Liu *et al.*, 2005). Taken together with the fact that propofol has been reported to have a very minor analgesic effect (Grounds *et al.*, 1987; Steinbacher, 2001), propofol sedation is regarded as appropriate for detecting the brain activation underlying pain perception in model animals. In fact, a previous study using fMRI under propofol sedation showed the changes in brain activity that underlie hypersensitivity to thermal stimulation (cold) after a peripheral nerve injury (Nagasaka *et al.*, 2017). In the present fMRI experiment, brain activity was increased in several brain areas under conditions in which mechanical and thermal stimuli evoking mechanical allodynia and thermal hyperalgesia, respectively, were applied. It is important to consider muscimol inactivation because it confirms that the increased activity observed in the animal under

anesthesia was involved in the allodynia and hyperalgesia seen during wakefulness. fMRI under propofol anesthesia could have utility for measuring the brain activity associated with pain and the effects of analgesic agents in animals.

4-4-2. Abnormal activation of the ACC, IC and SII

The present fMRI study suggested that neural activities in the ACC, IC, and SII underlie CPSP, as the activity of these areas significantly increased in association with mechanical allodynia and thermal hyperalgesia after VPL lesion. These activations are consistent with a meta-analysis of pain-related brain activity in healthy subjects and patients with abnormal pain after peripheral nerve injury and brainstem stroke (Lanz *et al.*, 2011). A case report of a single patient with CPSP 6 months following thalamic hemorrhage noted increased activity of the ACC and somatosensory cortices of the ipsi-lesional hemisphere on application of stimuli that evoked painful cold sensations (Seghier *et al.*, 2005). The fMRI results of the present study, regarding the activity in the ACC of the same subjects pre- and post-lesion, supports the case report in suggesting that this area is involved in the pathophysiology of CPSP. An important next step would be to investigate time-dependent changes in such activity following VPL lesion.

Here, I performed an inactivation study to confirm that there was a causal

relationship between the increased activity of the ACC and pain-like behavior in the macaque. Similar results were found in a recent study that verified the causal relationship between activation of the ACC and pain-related perceptions by demonstrating that formalin-evoked nociceptive behavior was reduced by optogenetic activation of inhibitory neurons in the ACC of mice (Gu *et al.*, 2015). Furthermore, anterior cingulotomy has been shown to be effective in the management of intractable pain (Ballantine *et al.*, 1967; Yen *et al.*, 2005; Sharim & Pouratian, 2016). According to the present fMRI results, the location of the cluster showing activation within the ACC corresponded to the anterior subdivision of that structure, which receives projections from thalamic MD neurons (Dum *et al.*, 2009). Previous studies in animals showed that the excitatory synaptic transmission at the fibers that connect MD neurons with the pyramidal cells in the ACC is increased after nerve injury (Li *et al.*, 2010; Koga *et al.*, 2015). As this finding was derived from rodent models of peripheral or spinal cord injury, it is important to determine whether the same plastic changes in neurons occur in the pathway between the ACC and MD in the present macaque CPSP model.

It was not possible to verify whether both the IC and SII are involved in allodynia or hyperalgesia in this study because the inactivation achieved using muscimol inactivated both areas. However, an MRI study using voxel-based morphometry (VBM)

analysis in CPSP patients revealed a decrease in gray matter volume in the pain processing areas, including both the IC and SII. Moreover, an fMRI experiment done on a monkey with neuropathic pain caused by peripheral neuropathy reported that activation of both the IC and the SII was associated with hypersensitivity to cold stimulation (Nagasaka *et al.*, 2017). These findings indicate that plastic changes in both the IC and SII are key factors underlying neuropathic pain. A previous study using rats that had undergone peripheral nerve ligation showed that increased excitatory synaptic transmission in the neurons of the IC was triggered by enhanced signaling of the AMPA receptor (*i.e.*, the non-N-methyl-d-aspartate subtype of the glutamate receptor) and involved neuropathic pain (Qiu *et al.*, 2014). Furthermore, manipulation of GABA neurotransmission in the IC can alter the pain threshold and lead to the development of analgesia or hyperalgesia (Jasmin *et al.*, 2003). These observations suggest that dysfunction of inhibitory or excitatory neurons in the IC/SII is involved in the allodynia and hyperalgesia seen in CPSP.

Plastic changes involving abnormal activity in cortical regions may occur not only in these cortical neurons, but also in thalamic neurons in the area surrounding the lesioned VPL. Accumulating evidence from post-stroke animal models has suggested that there are changes in dendritic spine shape or length in the area surrounding a lesion (Yuste

& Majewska, 2001; Brown *et al.*, 2008) and that the changes in the spine are associated with the stimulation of excitatory synaptic activity (Korkotian & Segal, 1999). Therefore, in the CPSP macaque model, the regions surrounding the lesioned VPL may have been affected by the changes in the spine, and this may have enhanced the excitatory transmission involving the spino–thalamo–cortical pathway. Importantly, the locations of the clusters showing activation within the ACC, IC, and SII on fMRI (*i.e.*, inactivation sites) corresponded to regions receiving projections from the MD, posterior part of the ventral medial nucleus (VMpo), and ventral posterior inferior nucleus (VPI), respectively (Craig, 2004; Dum *et al.*, 2009). These thalamic subdivisions are known to be the termination points of spinothalamic tracts and are located near the lesioned VPL (Dum *et al.*, 2009). Hence, plasticity of the spine was evident in these thalamic nuclei and may have contributed to the abnormal activity of the anatomically connected areas. By using the macaque model of CPSP, it will be possible to identify the cellular changes underlying increased activity observed in the present fMRI analysis.

4-5. Figures and figure legends

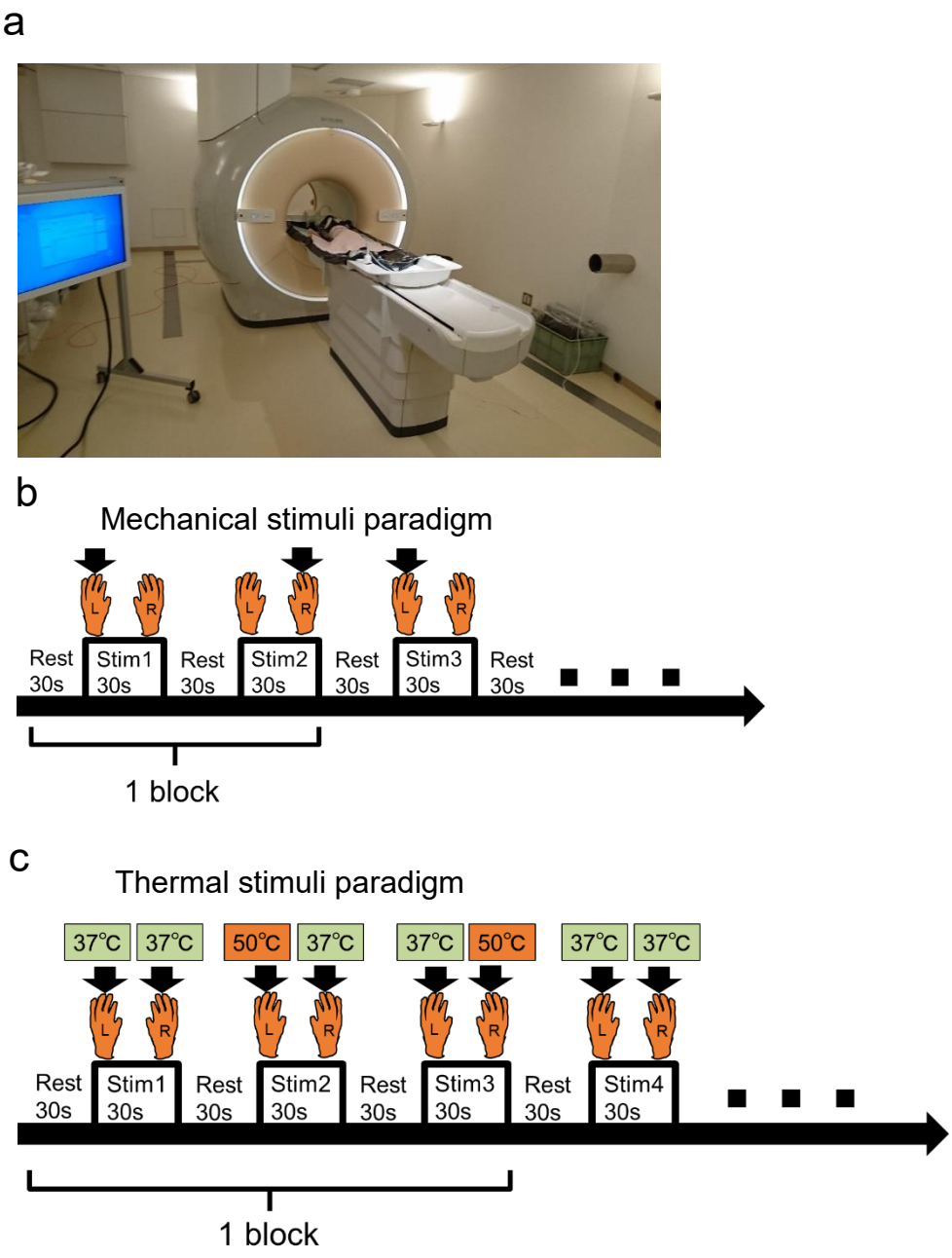

Figure 9. Block design of the fMRI experiment. (**a**) A standard 3.0 T MRI scanner was used to measure brain activity. The experimenter delivered mechanical and thermal stimuli to the monkey's hand according to the instructions on the screen to the left of the

figure. (**b**) The experiment using the mechanical stimuli paradigm employed a block design with two conditions, each of which lasted for 30 s: mechanical stimulation of the right and left hand (indicated by arrows). (**c**) The experiment using the thermal stimuli paradigm employed a block design with three conditions, each of which lasted 30 s: (1) 37°C control stimulation of both the right and left hands; (2) 50°C thermal stimulation of the right hand and 37°C stimulation of the left hand; and (3) 50°C thermal stimulation of the left hand and 37°C stimulation of the right hand.

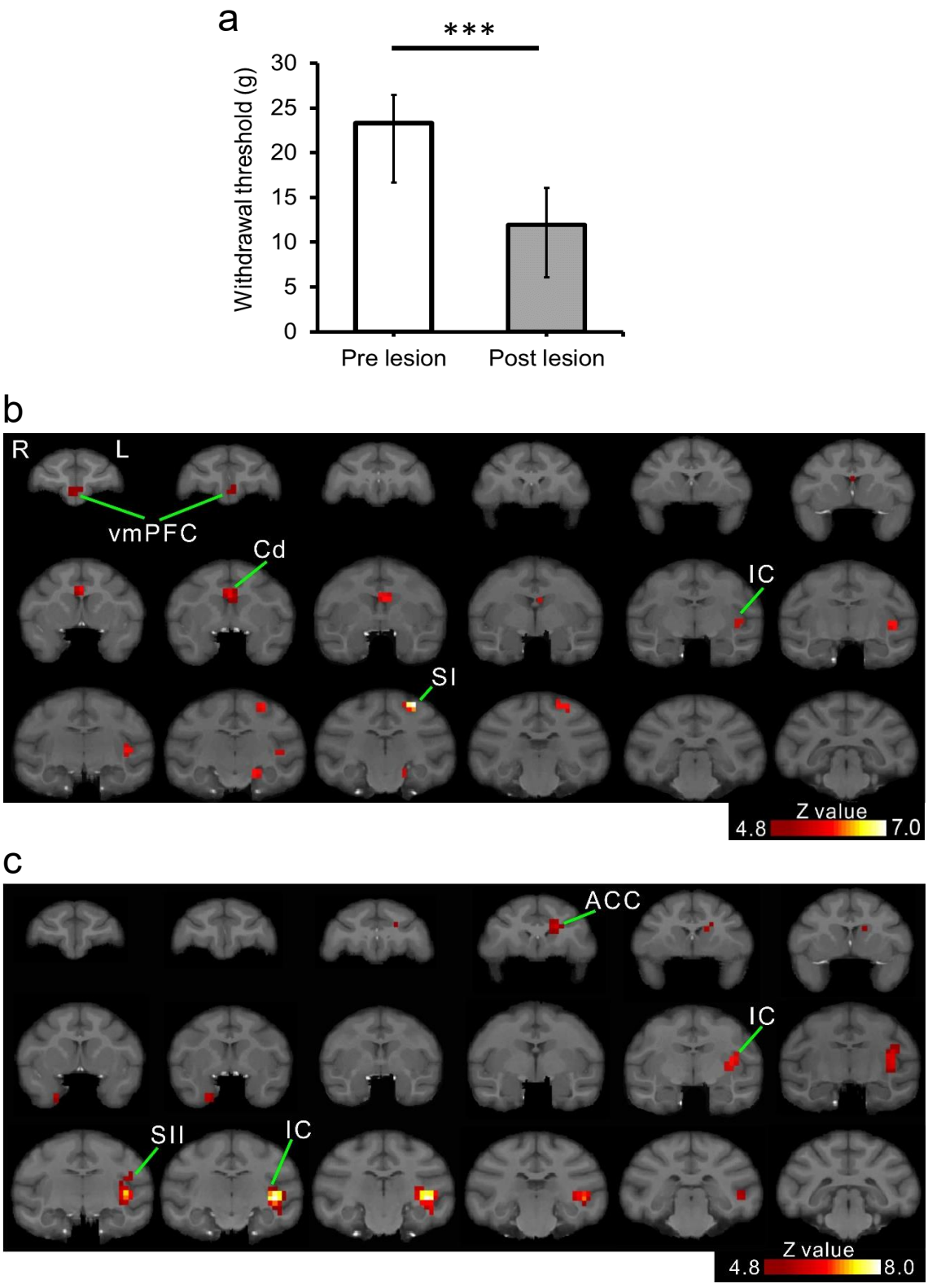
a
***
Withdrawal threshold (g)
30
25
20
15
10
5
0
Pre lesion
Post lesion
b
R
L
vmPFC
Cd
IC
SI
Z value
4.8
7.0
c
ACC
IC
SII
IC
Z value
4.8
8.0

Figure 10. Changes in brain activity associated with mechanical allodynia. (**a**) At least 3 months following the VPL lesion (post-lesion), the monkey demonstrated mechanical allodynia; the withdrawal threshold in response to the mechanical stimulation was significantly decreased compared with before the lesion (***$P < 0.001$, Mann–Whitney U test). Values are expressed as medians and interquartile ranges. Brain activity associated with mechanical stimulation (*i.e.,* activity during stimulus application to the right hand minus that during stimulus application to the left hand) during pre-lesion (**b**) and post-lesion period (**c**); calculations were performed using SPM12, and the statistical map was superimposed on the macaque template brain. Statistical significance was set at $P < 0.01$ (corrected for multiple comparisons) and the minimum cluster size was five voxels. The z-scores are represented on a color scale. Key areas of activation are indicated by the following abbreviations: ACC, anterior cingulate cortex; Cd, caudate nucleus; IC, insular cortex; SI, primary somatosensory cortex; SII, secondary somatosensory cortex; and vmPFC, ventromedial prefrontal cortex. In (**b**) and (**c**), a series of coronal images obtained at 2 mm intervals are arranged from rostral (upper-left, y = 22) to caudal (lower-right, y = -12). The “L” inserted in Figure **b** refers to the left. *i.e.*, the lesioned, hemisphere.

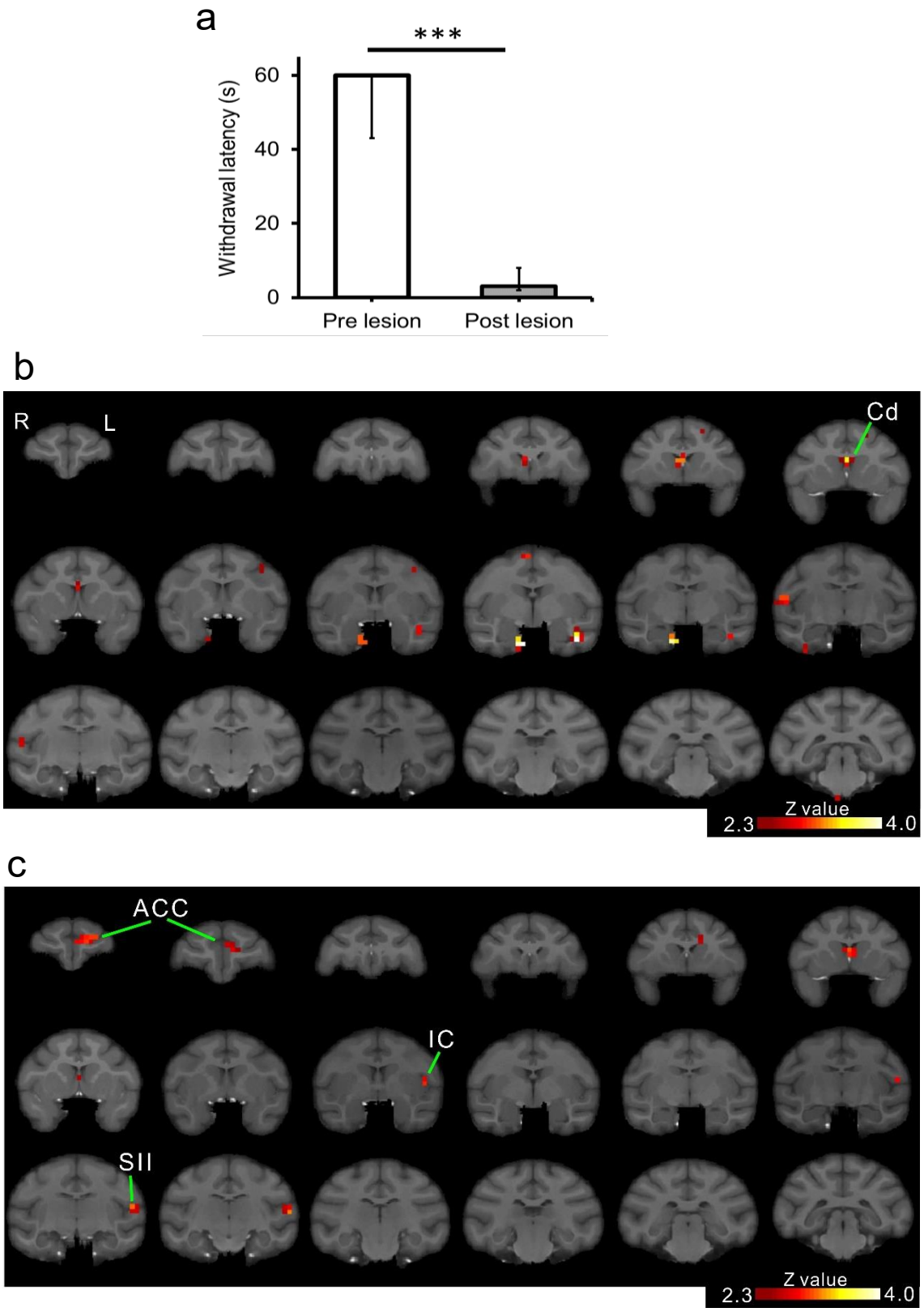
a
***
Withdrawal latency (s)
60
40
20
0
Pre lesion
Post lesion
b
R
L
Cd
Z value
2.3
4.0
c
ACC
IC
SII
Z value
2.3
4.0

Figure 11. Changes in brain activity associated with thermal hyperalgesia. (**a**) At least 3 months following VPL lesion (post-lesion), the monkey demonstrated thermal hyperalgesia; the withdrawal latency in response to the thermal stimulation (50°C) was significantly decreased compared with that before the lesion (***$P < 0.001$, Mann–Whitney U test). Increased brain activity associated with thermal stimulation (*i.e.*, the activity at 50°C thermal stimulation minus that at 37°C control stimulation) during pre-lesion (**b**) and post-lesion period (**c**); calculations were performed using SPM12, and the statistical map was superimposed on the macaque template brain. The statistical results were thresholded at $P < 0.01$ (uncorrected) and the minimum cluster size was four voxels. The z-scores are represented on a color scale. Key areas of activation are indicated by the following abbreviations: ACC, anterior cingulate cortex; Cd, caudate nucleus; IC, insular cortex; SII, secondary somatosensory cortex. In (**b**) and (**c**), a series of coronal images obtained at 2 mm intervals are arranged from rostral (upper-left, y = 22) to caudal (lower-right, y = -12). The "L" inserted in Figure **b** refers to the left hemisphere, which corresponds to the lesioned hemisphere.

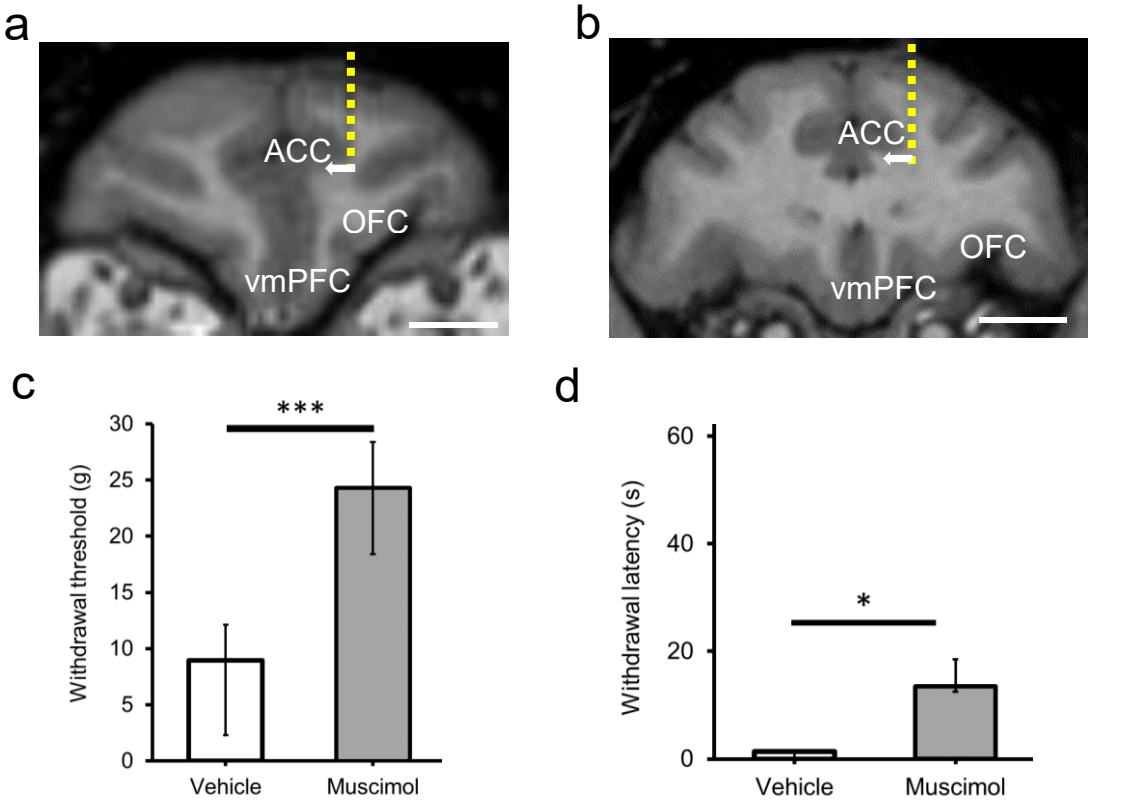

Figure 12. Effect of inactivation of the ACC on mechanical allodynia and thermal hyperalgesia. (**a**, **b**) Coronal MR images show muscimol injection sites of the ACC. The yellow dotted lines indicate the needle track, and the arrows indicate the direction of muscimol diffusion. The two injection sites were separated by 5 mm in a rostrocaudal direction. Scale bars = 10 mm. ACC, anterior cingulate cortex; OFC, orbital frontal cortex; vmPFC, ventromedial prefrontal cortex. (**c**, **d**) Muscimol injection into the ACC in the macaque 6 months after the lesion significantly increased the withdrawal threshold in response to mechanical stimulation (**c**) and the withdrawal latency in response to thermal (50°C) stimulation (**d**) compared with the vehicle control (*$P < 0.05$ and ***$P < 0.001$, Mann–Whitney U test). Values are expressed as medians and interquartile ranges.

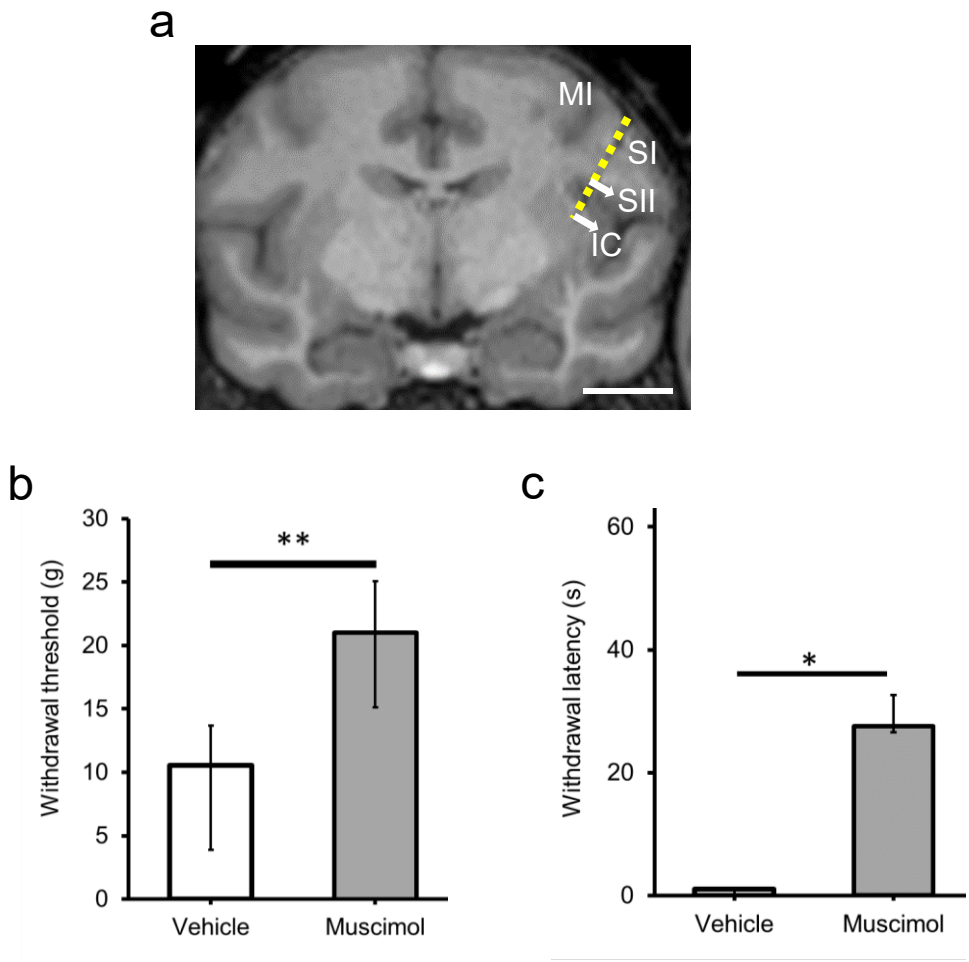

Figure 13. Effect of inactivation of the IC/SII on mechanical allodynia and thermal hyperalgesia. (**a**) Coronal MRI shows muscimol injection sites of the IC and SII. The yellow dotted line indicates the needle track, and the arrows indicate the direction of muscimol diffusion. The two injection sites were separated by 5 mm in a depth direction. Scale bar = 10 mm. IC, insular cortex; SII, secondary somatosensory cortex; MI, primary motor cortex. (**b**, **c**) Muscimol injection into IC/SII in the macaque 6 months following the lesion significantly increased the withdrawal threshold in response to mechanical

stimulation, and the withdrawal latency in response to thermal (50°C) stimulation, compared with the vehicle control (*$P < 0.05$ and **$P < 0.01$, Mann–Whitney U test). Values are expressed as medians and interquartile ranges.

4-6. Tables

Table 2. Brain regions showing significant increased brain activity during mechanical stimulation at pre lesion and post lesion.

Area	Hemisphere	Z score	x	y	z (mm)
Pre lesion (right hand stimulation－left hand stimulation)					
SI	L	6.61	10	-14	20
Cd	B	6.16	2	2	8
IC	L	5.81	20	-4	-2
Hip	L	5.76	12	-10	-10
PFC	B	5.17	2	16	4
Post lesion (right hand stimulation－left hand stimulation)					
IC	L	Inf.	16	-4	4
VII	R	6.55	-10	-40	4
ACC	L	5.76	4	10	10
PRH	R	5.50	-10	2	-14

The locations are indicated with the positions along the x (left-right), y (rostro-caudal) and z (dorso-ventral) axes of the Horsley-Clarke stereotaxic coordinates. ACC, anterior cingulate cortex; Cd, caudate nucleus; Hip, hipocammpus; IC, insular cortex; PFC, prefrontal cortex; PRH, perirhinal cortex; SI, primary somatosensory cortex; VII, secondary visual cortex; L, left hemisphere (ipsi-lesional hemisphere); R, Right hemisphere (contra-lesional hemisphere); B, bilateral hemisphere; Inf, Infinity.

Table 3. Brain regions showing significant increased brain activity during thermal stimulation at pre lesion and post lesion.

Area	Hemisphere	Z score	x	y	z (mm)
Pre lesion (R50/L37－R37/L37)					
TC	L	3.63	18	-2	-14
EC	R	3.62	-10	-2	-14
Cd	B	3.22	0	6	6
IP	L	3.07	8	-28	20
VI	R	3.02	-10	-40	10
IP	R	2.93	-8	-28	10
SII	R	2.91	-24	-8	4
VII	L	2.84	8	-34	-2
Post lesion (R50/L37－R37/L37)					
OFC	R	4.05	-8	20	6
VI	L	3.83	16	-38	-4
SII	L	3.04	24	-8	2
IP	L	2.99	12	-22	18
Sep	B	2.89	0	4	6
ACC	L	2.88	2	16	10
IC	L	2.79	18	0	2
VI	R	2.54	-14	-40	-2

The locations are indicated with the positions along the x (left-right), y (rostro-caudal) and z (dorso-ventral) axes of the Horsley-Clarke stereotaxic coordinates. ACC, anterior

cingulate cortex; Cd, caudate nucleus; EC, entorhinal cortex; IC, insular cortex; IP, intraparietal cortex; OFC, orbital frontal cortex; TC, interotemporal cortex; SII, secondary somatosensory cortex; VI, praimary visual cortex; VII, secondary visual cortex; L, left hemisphere (ipsi-lesional hemisphere); R, Right hemisphere (contra-lesional hemisphere); B, bilateral hemisphere.

Chapter 5. General discussion

Neuropathic pain is defined as “pain caused by a lesion or disease of the somatosensory system” (www.iasp-pain.org/resources/painDefinition). Traditionally, to investigate the underlying mechanisms, studies of neuropathic pain have been performed in model animals after peripheral nerve and spinal cord injury. Several studies show that plastic changes involving the pathophysiology of neuropathic pain occurred not only around the injured area but also in areas distant from the site of the lesion. For example, a recent study indicates that peripheral nerve injury enhanced excitatory synaptic transmission in the ACC in the brain (Koga *et al.*, 2015). Moreover, inflammatory changes associated with plasticity or electrophysiological alterations are observed in areas of the brain associated with pain processing, such as the thalamus and multiple neocortical areas, after spinal cord injury (Zhao *et al.*, 2007; Yoon *et al.*, 2013). These observations suggest that plastic changes involved in neuropathic pain occur in a wide range of pain-related brain areas. Furthermore, several studies have indicated that changes in brain activity in subjects following nerve injury differ between individuals with and without abnormal pain (Willoch *et al.*, 2004; Ducreux *et al.*, 2006; Casey *et al.*, 2012). Thus, investigation of plasticity is crucial to elucidate the mechanism of abnormal pain and to develop novel

treatments, such as drugs.

CPSP is also caused by lesions of the somatosensory pathways, and it has been suggested to be caused by plasticity of neural systems, such as peripheral nerves (Takami *et al.*, 2011) and the brain (Kuan *et al.*, 2015). To study the mechanisms of CPSP, this study focused on plasticity in the brain because it is considered to be the center of pain processing (Chen, 2009). Previously, animal models of CPSP have been developed using rodents (Wasserman & Koeberle, 2009; Hanada *et al.*, 2014). However, areas involved in pain processing in humans do not exist in rodents (Kaas, 2004; Wallis, 2012). Therefore, Experiment 1 was performed to develop a new animal model of CPSP using the rhesus macaque whose brain shows homology with the human brain.

Several clinical investigations indicated that CPSP is caused by hemorrhagic or ischemic lesions of the lateral spinothalamic tract and its terminations (Montes *et al.*, 2005; Kumar *et al.*, 2009; Krause *et al.*, 2012; Sprenger *et al.*, 2012; Hosomi *et al.*, 2015). The thalamic VPL (known as the termination of the lateral spinothalamic tract) is the most common lesion site causing CPSP (Krause *et al.*, 2012), and the thalamus shows a predilection for hemorrhage in humans (Fewel *et al.*, 2003). Therefore, a hemorrhagic VPL lesion was used to develop a macaque model of CPSP in this study.

The results of Experiment 1 indicated behavioral changes in lesioned macaques,

indicating the occurrence of both mechanical allodynia and thermal hyperalgesia several weeks after the lesion. In contrast, several studies in rodent hemorrhagic VPL lesion models indicated that the behavioral changes occurred within 1 week after the lesion (Wasserman & Koeberle, 2009; Castel *et al.*, 2013; Hanada *et al.*, 2014). The majority of patients with CPSP begin to complain of abnormal pain following a delay of several weeks after a stroke (Kumar *et al.*, 2009). Thus, the present model using macaques reproduced the symptoms of CPSP patients more faithfully than have other experimental animal models. The difference between the present and previous models is considered to reflect species differences or differences in the size and location of the lesion. As the macaque model showed a long interval without abnormal pain after the lesion, this model is better for studying pre-emptive pharmacological treatments compared to rodent models.

In Experiment 2, histological changes in the glial cells and neuronal degeneration in the perilesional area of the present macaque model were investigated. Immunohistochemical analyses confirmed the presence of activated microglia and astrocytes in the perilesional and lesional areas at 3 months after the lesion. The results of Experiment 2 indicated activated microglia and astrocytes in the area surrounding surviving neurons in the perilesional area; therefore, these glial cells may enhance the excitability of neurons through some molecular pathways (Jarvis, 2010; Ferrini & De

Koninck, 2013). Brain-derived neurotrophic factor (BDNF), which is released by activated glial cells, is a neuromodulator and is crucial for neural plasticity (Abidin *et al.*, 2008; Thibault *et al.*, 2014). Several lines of evidence indicate that BDNF not only induces morphological alterations such as dendrite number and axon complexity but also enhances neuronal excitability (Danzer *et al.*, 2002; Tolwani *et al.*, 2002; Langhammer *et al.*, 2010; Thibault *et al.*, 2014). The long-lasting glial activation confirmed in the macaque model likely affects surviving neurons in the perilesional area, some of which convey noxious information (Apkarian & Shi, 1994). Hanada et al. (2014) showed that abnormal pain in CPSP mouse models is reduced by infusion of minocycline, which is known to attenuate activation of microglia, and they suggested that the activated glial cells play an important role in the pathophysiology of CPSP. This inhibitor may act on abnormal pain by suppression of BDNF release. Thus, an important next step is to assess whether the administration of minocycline or BDNF can reduce or increase pain-related behavior and brain activity in the present macaque model. In contrast to the macaque CPSP model, previous studies in rodent CPSP models confirmed the presence of activated glial cells in the perilesional area up to 1 month after induction of the lesion (Wasserman & Koeberle, 2009; Hanada *et al.*, 2014). Hence, the present model may also have an advantage over other experimental models in testing therapeutic interventions that last for

several months, such as continuous pharmacological treatment and rehabilitative training.

Experiment 3 confirmed the involvement of increased brain activities in the ACC, IC, and SII with mechanical allodynia and thermal hyperalgesia by a combination of fMRI with muscimol inactivation. The macaques used in this experiment were sedated by continuous intravenous infusion of propofol during fMRI scanning to remove motion artifacts, which could confound detection of brain activities involved in pain. However, as described in the Discussion in Experiment 3, propofol has been reported to have a low analgesic effect (Grounds *et al.*, 1987; Steinbacher, 2001), so propofol sedation is regarded as being appropriate to detect brain activation patterns that underlie pain perception in animals (Nagasaka *et al.*, 2017). In fact, the present experiment successfully demonstrated that brain activity changes in the ACC, IC, and SII associated with CPSP could be measured by fMRI in the sedated macaque model. The activity changes were consistent with those of brain imaging studies in human patients with CPSP (Seghier *et al.*, 2005). The present results suggested that brain activity measured by fMRI combined with behavioral outcomes in macaques could be used to further understand the mechanism of CPSP.

Obviously, animal models of CPSP have a number of limitations: (1) Animals do not report their sensation as humans do. In animal experiments, it is difficult to clearly

determine whether increased withdrawal responses are due to pain perception or other symptoms (e.g., increased spinal reflexes after stroke). In the present experiments, however, as the withdrawal response of macaque was decreased due to pharmacological inactivation of increased brain activity often found in neuropathic pain patients (Seghier *et al.*, 2005), there was at least a relationship between the behavioral response and the changes in pain-related brain activity. Therefore, the developed model may evaluate the animals' pain perception and effects of therapeutic interventions better than other experimental models reported previously. (2) Quantitative evaluation of spontaneous pain is difficult in animals. It is known that patients with CPSP commonly present with spontaneous pain as well as evoked pain (Leijon *et al.*, 1989; Andersen *et al.*, 1995). Interestingly, a previous brain imaging study indicated functional connectivity between the nucleus accumbens (NAc) and medial PFC (mPFC) in chronic pain patients, and showed a correlation between the strength of NAc-mPFC connectivity and reported magnitude of spontaneous pain (Baliki *et al.*, 2010). Thus, the degree of spontaneous pain could be assessed by analysis of the connectivity. The functional connectivity has been evaluated using fMRI data, but there have been no reports adapting it to CPSP (Hosomi *et al.*, 2015). Therefore, further imaging studies are required to investigate how changes in functional connectivity are involved in CPSP and to determine the strength of NAc–

mPFC connectivity. (3) The dorsolateral prefrontal cortex (DLPFC) is crucial for the functions of working memory (Owen *et al.*, 1996; Petrides, 2000; Koechlin *et al.*, 2003) and emotional regulation (Phillips *et al.*, 2008; Wager *et al.*, 2008). Atrophy of the DLPFC related to duration of pain has been reported in human patients with chronic pain (Apkarian *et al.*, 2004). Thus, this region may also be involved in the pathology of CPSP. On the other hand, megascopic anatomical study of DLPFC indicated interspecies anatomical differences between humans and macaques (Petrides *et al.*, 2012). These discrepancies could be overcome by comparing experimental results in the macaque model obtained by functional and anatomical neuroimaging with those of human patients.

To eliminate pain, several nonpharmacological therapies, such as neuromodulation and neurostimulation approaches, have been administered in patients with aggravated CPSP (Migita *et al.*, 1995; Lefaucheur *et al.*, 2001). Repetitive transcranial magnetic stimulation (rTMS) is a noninvasive approach to induce electric currents in the cortex through the scalp, and the analgesic effect of high-frequency rTMS (≥5Hz) of MI has been confirmed in approximately 40% of patients with CPSP (Hosomi *et al.*, 2015). The mechanisms underlying the analgesic effect are still unclear. Using the CPSP macaque model, which has a large brain relative to rodent models, with a combination of behavioral outcome monitoring and fMRI may contribute to determining

the mechanisms underlying the analgesic effect seen with rTMS of MI and validating more effective stimulation sites and stimulation frequencies.

The current macaque model replicated the symptoms seen in human CPSP patients, and could therefore contribute to closing the translational gap between preclinical and clinical pain research.

List of Abbreviations

ACC: anterior cingulate cortex

BDNF: brain-derived neurotrophic factor

BOLD: blood oxygenation level-dependent

Cd: caudate nucleus

CM: central medial nucleus

CPSP: central post-stroke pain

DLPFC: dorsolateral prefrontal cortex

EPI: echo-planar imaging

EC: entorhinal cortex

fMRI: functional magnetic resonance imaging

GABA: γ-aminobutyric acid

GFAP: glial fibrillary acidic protein

GLd: dorsal lateral geniculate nucleus

Hip: hippocampus

Iba-1: ionized calcium binding adaptor molecule 1

IC: insular cortex

IL: interleukin

IP: intraparietal cortex

KCC2: K-Cl cotransporter

MD: mediodorsal nucleus

MI: primary motor cortex

mPFC: medial prefrontal cortex

MRI: magnetic resonance imaging

NAc: nucleus accumbens

NeuN: neuronal nuclear antigen

NEX: number of excitations

LD: lateral dorsal nucleus

LP: lateral posterior nucleus

LTP: long term-potentiation

OD: optical density

OFC: orbital frontal cortex

PET: positron emission tomography

PFC: prefrontal cortex

PRH: perirhinal cortex

Pul: pulvinar nucleus

R: reticular nucleus

rTMS: repetive transcranial magnetic stimulation

Sep: septum

SG: suprageniculate nucleus

SI: primary somatosensory cortex

SII: secondary somatosensory cortex

TC: interotemporal cortex

TE: echo time

TR: repetition time

VBM: voxel-based morphometry

VI: primary visual cortex

VII: secondary visual cortex

VMpo: ventral medial posterior nucleus

vmPFC: ventromedial prefrontal cortex

VPI: ventral posteroinferior nucleus

VLc: caudal part of the ventrolateral nucleus

VLo: oral part of the ventrolateral nucleus

VLps: ventrolateral nucleus, pars postrema

VPL: ventral posterolateral nucleus

VPM: ventral posteromedial nucleus

VPS: ventroposterior superior nucleus

References

Abidin, I., Eysel, U.T., Lessmann, V. & Mittmann, T. (2008) Impaired GABAergic inhibition in the visual cortex of brain-derived neurotrophic factor heterozygous knockout mice. *J Physiol*, **586**, 1885-1901.

Almeida, T.F., Roizenblatt, S. & Tufik, S. (2004) Afferent pain pathways: a neuroanatomical review. *Brain Res*, **1000**, 40-56.

Andersen, G., Vestergaard, K., Ingeman-Nielsen, M. & Jensen, T.S. (1995) Incidence of central post-stroke pain. *Pain*, **61**, 187-193.

Andersson, J.L., Lilja, A., Hartvig, P., Langstrom, B., Gordh, T., Handwerker, H. & Torebjork, E. (1997) Somatotopic organization along the central sulcus, for pain localization in humans, as revealed by positron emission tomography. *Exp Brain Res*, **117**, 192-199.

Antognini, J.F., Buonocore, M.H., Disbrow, E.A. & Carstens, E. (1997) Isoflurane anesthesia blunts cerebral responses to noxious and innocuous stimuli: a fMRI study. *Life Sci*, **61**, PL 349-354.

Apkarian, A.V. (2011) The brain in chronic pain: clinical implications. *Pain Manag*, **1**, 577-586.

Apkarian, A.V., Bushnell, M.C., Treede, R.D. & Zubieta, J.K. (2005) Human brain mechanisms of pain perception and regulation in health and disease. *Eur J Pain*, **9**, 463-484.

Apkarian, A.V. & Hodge, C.J. (1989) Primate spinothalamic pathways: III. Thalamic terminations of the dorsolateral and ventral spinothalamic pathways. *J Comp Neurol*, **288**, 493-511.

Apkarian, A.V. & Shi, T. (1994) Squirrel monkey lateral thalamus. I. Somatic nociresponsive neurons and their relation to spinothalamic terminals. *J Neurosci*,

14, 6779-6795.

Apkarian, A.V., Sosa, Y., Sonty, S., Levy, R.M., Harden, R.N., Parrish, T.B. & Gitelman, D.R. (2004) Chronic back pain is associated with decreased prefrontal and thalamic gray matter density. *J Neurosci*, **24**, 10410-10415.

Armstrong, D.M. (1988) The supraspinal control of mammalian locomotion. *J Physiol*, **405**, 1-37.

Baliki, M.N., Geha, P.Y., Fields, H.L. & Apkarian, A.V. (2010) Predicting value of pain and analgesia: nucleus accumbens response to noxious stimuli changes in the presence of chronic pain. *Neuron*, **66**, 149-160.

Ballantine, H.T., Jr., Cassidy, W.L., Flanagan, N.B. & Marino, R., Jr. (1967) Stereotaxic anterior cingulotomy for neuropsychiatric illness and intractable pain. *J Neurosurg*, **26**, 488-495.

Bastos, L.F., de Oliveira, A.C., Watkins, L.R., Moraes, M.F. & Coelho, M.M. (2012) Tetracyclines and pain. *Naunyn Schmiedebergs Arch Pharmacol*, **385**, 225-241.

Berthier, M., Starkstein, S. & Leiguarda, R. (1988) Asymbolia for pain: a sensory-limbic disconnection syndrome. *Ann Neurol*, **24**, 41-49.

Black, K.J., Koller, J.M., Snyder, A.Z. & Perlmutter, J.S. (2004) Atlas template images for nonhuman primate neuroimaging: baboon and macaque. *Methods in enzymology*, **385**, 91-102.

Blasi, F., Herisson, F., Wang, S., Mao, J. & Ayata, C. (2015) Late-onset thermal hypersensitivity after focal ischemic thalamic infarcts as a model for central post-stroke pain in rats. *J Cereb Blood Flow Metab*, **35**, 1100-1103.

Bliss, T.V., Collingridge, G.L., Kaang, B.K. & Zhuo, M. (2016) Synaptic plasticity in the anterior cingulate cortex in acute and chronic pain. *Nat Rev Neurosci*, **17**, 485-496.

Bowsher, D. (1995) The management of central post-stroke pain. *Postgrad Med J*, **71**,

598-604.

Bowsher, D. (2005) Allodynia in relation to lesion site in central post-stroke pain. *J Pain*, **6**, 736-740.

Brooks, J. & Tracey, I. (2005) From nociception to pain perception: imaging the spinal and supraspinal pathways. *J Anat*, **207**, 19-33.

Brown, C.E., Wong, C. & Murphy, T.H. (2008) Rapid morphologic plasticity of peri-infarct dendritic spines after focal ischemic stroke. *Stroke*, **39**, 1286-1291.

Bushnell, M.C., Ceko, M. & Low, L.A. (2013) Cognitive and emotional control of pain and its disruption in chronic pain. *Nat Rev Neurosci*, **14**, 502-511.

Bushnell, M.C., Duncan, G.H., Hofbauer, R.K., Ha, B., Chen, J.I. & Carrier, B. (1999) Pain perception: is there a role for primary somatosensory cortex? *Proc Natl Acad Sci U S A*, **96**, 7705-7709.

Carstens, E., Leah, J., Lechner, J. & Zimmermann, M. (1990) Demonstration of extensive brainstem projections to medial and lateral thalamus and hypothalamus in the rat. *Neuroscience*, **35**, 609-626.

Casey, K.L., Geisser, M., Lorenz, J., Morrow, T.J., Paulson, P. & Minoshima, S. (2012) Psychophysical and cerebral responses to heat stimulation in patients with central pain, painless central sensory loss, and in healthy persons. *Pain*, **153**, 331-341.

Castel, A., Helie, P., Beaudry, F. & Vachon, P. (2013) Bilateral central pain sensitization in rats following a unilateral thalamic lesion may be treated with high doses of ketamine. *BMC Vet Res*, **9**, 59.

Castel, A. & Vachon, P. (2013) Gabapentin reverses central pain sensitization following a collagenase-induced intrathalamic hemorrhage in rats. *J Pain Res*, **7**, 5-12.

Chen, A.C. (2009) Higher cortical modulation of pain perception in the human brain: Psychological determinant. *Neurosci Bull*, **25**, 267-276.

Craig, A.D. (2004) Distribution of trigeminothalamic and spinothalamic lamina I terminations in the macaque monkey. *J Comp Neurol*, **477**, 119-148.

Craig, A.D. (2008) Retrograde analyses of spinothalamic projections in the macaque monkey: input to the ventral lateral nucleus. *J Comp Neurol*, **508**, 315-328.

Danzer, S.C., Crooks, K.R., Lo, D.C. & McNamara, J.O. (2002) Increased expression of brain-derived neurotrophic factor induces formation of basal dendrites and axonal branching in dentate granule cells in hippocampal explant cultures. *J Neurosci*, **22**, 9754-9763.

Dietz, V. (2012) Neuronal plasticity after a human spinal cord injury: positive and negative effects. *Exp Neurol*, **235**, 110-115.

Dimyan, M.A. & Cohen, L.G. (2011) Neuroplasticity in the context of motor rehabilitation after stroke. *Nat Rev Neurol*, **7**, 76-85.

Doyen, P.J., Vergouts, M., Pochet, A., Desmet, N., van Neerven, S., Brook, G. & Hermans, E. (2017) Inflammation-associated regulation of RGS in astrocytes and putative implication in neuropathic pain. *J Neuroinflammation*, **14**, 209.

Ducreux, D., Attal, N., Parker, F. & Bouhassira, D. (2006) Mechanisms of central neuropathic pain: a combined psychophysical and fMRI study in syringomyelia. *Brain*, **129**, 963-976.

Dum, R.P., Levinthal, D.J. & Strick, P.L. (2009) The spinothalamic system targets motor and sensory areas in the cerebral cortex of monkeys. *J Neurosci*, **29**, 14223-14235.

Eroglu, C. & Barres, B.A. (2010) Regulation of synaptic connectivity by glia. *Nature*, **468**, 223-231.

Ferrini, F. & De Koninck, Y. (2013) Microglia control neuronal network excitability via BDNF signalling. *Neural Plast*, **2013**, 429815.

Fewel, M.E., Thompson, B.G., Jr. & Hoff, J.T. (2003) Spontaneous intracerebral hemorrhage: a review. *Neurosurg Focus*, **15**, E1.

Foltz, E.L. & White, L.E., Jr. (1962) Pain "relief" by frontal cingulumotomy. *J Neurosurg*, **19**, 89-100.

Francis, J.T., Xu, S. & Chapin, J.K. (2008) Proprioceptive and cutaneous representations in the rat ventral posterolateral thalamus. *J Neurophysiol*, **99**, 2291-2304.

Garraghty, P.E., Florence, S.L. & Kaas, J.H. (1990) Ablations of areas 3a and 3b of monkey somatosensory cortex abolish cutaneous responsivity in area 1. *Brain Res*, **528**, 165-169.

Greenspan, J.D., Lee, R.R. & Lenz, F.A. (1999) Pain sensitivity alterations as a function of lesion location in the parasylvian cortex. *Pain*, **81**, 273-282.

Greenspan, J.D., Ohara, S., Sarlani, E. & Lenz, F.A. (2004) Allodynia in patients with post-stroke central pain (CPSP) studied by statistical quantitative sensory testing within individuals. *Pain*, **109**, 357-366.

Grounds, R.M., Lalor, J.M., Lumley, J., Royston, D. & Morgan, M. (1987) Propofol infusion for sedation in the intensive care unit: preliminary report. *Br Med J (Clin Res Ed)*, **294**, 397-400.

Gu, L., Uhelski, M.L., Anand, S., Romero-Ortega, M., Kim, Y.T., Fuchs, P.N. & Mohanty, S.K. (2015) Pain inhibition by optogenetic activation of specific anterior cingulate cortical neurons. *PLoS One*, **10**, e0117746.

Hanada, T., Kurihara, T., Tokudome, M., Tokimura, H., Arita, K. & Miyata, A. (2014) Development and pharmacological verification of a new mouse model of central post-stroke pain. *Neurosci Res*, **78**, 72-80.

Hatanaka, N., Tokuno, H., Hamada, I., Inase, M., Ito, Y., Imanishi, M., Hasegawa, N., Akazawa, T., Nambu, A. & Takada, M. (2003) Thalamocortical and intracortical connections of monkey cingulate motor areas. *J Comp Neurol*, **462**, 121-138.

Higo, N., Oishi, T., Yamashita, A., Matsuda, K. & Hayashi, M. (2002) Northern blot and in situ hybridization analyses of MARCKS mRNA expression in the cerebral

cortex of the macaque monkey. *Cereb Cortex*, **12**, 552-564.

Higo, N., Oishi, T., Yamashita, A., Matsuda, K. & Hayashi, M. (2004) Cell type- and region-specific expression of neurogranin mRNA in the cerebral cortex of the macaque monkey. *Cereb Cortex*, **14**, 1134-1143.

Higo, N., Sato, A., Yamamoto, T., Nishimura, Y., Oishi, T., Murata, Y., Onoe, H., Yoshino-Saito, K., Tsuboi, F., Takahashi, M., Isa, T. & Kojima, T. (2010) SPP1 is expressed in corticospinal neurons of the macaque sensorimotor cortex. *J Comp Neurol*, **518**, 2633-2644.

Hirato, M., Watanabe, K.a. & Yoshimoto, Y. (2010) Study on neural activity of thalamic sensory nucleus and microstimulation effect in patients with central post–stroke pain. *Pain Research*, **25**, 27-35.

Hosomi, K., Seymour, B. & Saitoh, Y. (2015) Modulating the pain network--neurostimulation for central poststroke pain. *Nat Rev Neurol*, **11**, 290-299.

Hubner, C.A., Stein, V., Hermans-Borgmeyer, I., Meyer, T., Ballanyi, K. & Jentsch, T.J. (2001) Disruption of KCC2 reveals an essential role of K-Cl cotransport already in early synaptic inhibition. *Neuron*, **30**, 515-524.

Iannetti, G.D., Zambreanu, L., Wise, R.G., Buchanan, T.J., Huggins, J.P., Smart, T.S., Vennart, W. & Tracey, I. (2005) Pharmacological modulation of pain-related brain activity during normal and central sensitization states in humans. *Proc Natl Acad Sci U S A*, **102**, 18195-18200.

Ishida, A., Isa, K., Umeda, T., Kobayashi, K., Kobayashi, K., Hida, H. & Isa, T. (2016) Causal Link between the Cortico-Rubral Pathway and Functional Recovery through Forced Impaired Limb Use in Rats with Stroke. *J Neurosci*, **36**, 455-467.

Jarvis, M.F. (2010) The neural-glial purinergic receptor ensemble in chronic pain states. *Trends Neurosci*, **33**, 48-57.

Jasmin, L., Rabkin, S.D., Granato, A., Boudah, A. & Ohara, P.T. (2003) Analgesia and hyperalgesia from GABA-mediated modulation of the cerebral cortex. *Nature*,

424, 316-320.

Kaas, J.H. (2004) Evolution of the large, complex sensorimotor systems of anthropoid primates. *Int. J. Comp. Psychol.*, **17**, 34-52.

Kaas, J.H., Nelson, R.J., Sur, M., Dykes, R.W. & Merzenich, M.M. (1984) The somatotopic organization of the ventroposterior thalamus of the squirrel monkey, Saimiri sciureus. *J Comp Neurol*, **226**, 111-140.

Kenshalo, D.R., Jr., Chudler, E.H., Anton, F. & Dubner, R. (1988) SI nociceptive neurons participate in the encoding process by which monkeys perceive the intensity of noxious thermal stimulation. *Brain Res*, **454**, 378-382.

Kim, J.H., Greenspan, J.D., Coghill, R.C., Ohara, S. & Lenz, F.A. (2007) Lesions limited to the human thalamic principal somatosensory nucleus (ventral caudal) are associated with loss of cold sensations and central pain. *J Neurosci*, **27**, 4995-5004.

Kim, J.S. (1998) Delayed-onset ipsilateral sensory symptoms in patients with central poststroke pain. *Eur Neurol*, **40**, 201-206.

Kim, J.Y. & Bae, H.J. (2017) Spontaneous Intracerebral Hemorrhage: Management. *J Stroke*, **19**, 28-39.

Kleinschnitz, C., Schutz, A., Nolte, I., Horn, T., Frank, M., Solymosi, L., Stoll, G. & Bendszus, M. (2005) In vivo detection of developing vessel occlusion in photothrombotic ischemic brain lesions in the rat by iron particle enhanced MRI. *J Cereb Blood Flow Metab*, **25**, 1548-1555.

Klit, H., Finnerup, N.B., Andersen, G. & Jensen, T.S. (2011) Central poststroke pain: a population-based study. *Pain*, **152**, 818-824.

Klit, H., Finnerup, N.B. & Jensen, T.S. (2009) Central post-stroke pain: clinical characteristics, pathophysiology, and management. *Lancet Neurol*, **8**, 857-868.

Kniffki, K.D. & Mizumura, K. (1983) Responses of neurons in VPL and VPL-VL region

of the cat to algesic stimulation of muscle and tendon. *J Neurophysiol*, **49**, 649-661.

Koechlin, E., Ody, C. & Kouneiher, F. (2003) The architecture of cognitive control in the human prefrontal cortex. *Science*, **302**, 1181-1185.

Koga, K., Descalzi, G., Chen, T., Ko, H.G., Lu, J., Li, S., Son, J., Kim, T., Kwak, C., Huganir, R.L., Zhao, M.G., Kaang, B.K., Collingridge, G.L. & Zhuo, M. (2015) Coexistence of two forms of LTP in ACC provides a synaptic mechanism for the interactions between anxiety and chronic pain. *Neuron*, **85**, 377-389.

Korkotian, E. & Segal, M. (1999) Bidirectional regulation of dendritic spine dimensions by glutamate receptors. *Neuroreport*, **10**, 2875-2877.

Krause, T., Asseyer, S., Taskin, B., Floel, A., Witte, A.V., Mueller, K., Fiebach, J.B., Villringer, K., Villringer, A. & Jungehulsing, G.J. (2016) The Cortical Signature of Central Poststroke Pain: Gray Matter Decreases in Somatosensory, Insular, and Prefrontal Cortices. *Cereb Cortex*, **26**, 80-88.

Krause, T., Brunecker, P., Pittl, S., Taskin, B., Laubisch, D., Winter, B., Lentza, M.E., Malzahn, U., Villringer, K., Villringer, A. & Jungehulsing, G.J. (2012) Thalamic sensory strokes with and without pain: differences in lesion patterns in the ventral posterior thalamus. *J Neurol Neurosurg Psychiatry*, **83**, 776-784.

Kuan, Y.H., Shih, H.C., Tang, S.C., Jeng, J.S. & Shyu, B.C. (2015) Targeting P(2)X(7) receptor for the treatment of central post-stroke pain in a rodent model. *Neurobiol Dis*, **78**, 134-145.

Kumar, B., Kalita, J., Kumar, G. & Misra, U.K. (2009) Central poststroke pain: a review of pathophysiology and treatment. *Anesth Analg*, **108**, 1645-1657.

Ladeby, R., Wirenfeldt, M., Garcia-Ovejero, D., Fenger, C., Dissing-Olesen, L., Dalmau, I. & Finsen, B. (2005) Microglial cell population dynamics in the injured adult central nervous system. *Brain Res Brain Res Rev*, **48**, 196-206.

Lahti, K.M., Ferris, C.F., Li, F., Sotak, C.H. & King, J.A. (1999) Comparison of evoked

cortical activity in conscious and propofol-anesthetized rats using functional MRI. *Magnetic Resonance in Medicine*, **41**, 412-416.

Langeron, O., Vivien, B., Paqueron, X., Saillant, G., Riou, B., Coriat, P. & Lille, F. (1999) Effects of propofol, propofol-nitrous oxide and midazolam on cortical somatosensory evoked potentials during sufentanil anaesthesia for major spinal surgery. *Br J Anaesth*, **82**, 340-345.

Langhammer, C.G., Previtera, M.L., Sweet, E.S., Sran, S.S., Chen, M. & Firestein, B.L. (2010) Automated Sholl analysis of digitized neuronal morphology at multiple scales: Whole cell Sholl analysis versus Sholl analysis of arbor subregions. *Cytometry A*, **77**, 1160-1168.

Lanz, S., Seifert, F. & Maihofner, C. (2011) Brain activity associated with pain, hyperalgesia and allodynia: an ALE meta-analysis. *J Neural Transm (Vienna)*, **118**, 1139-1154.

Lefaucheur, J.P., Drouot, X. & Nguyen, J.P. (2001) Interventional neurophysiology for pain control: duration of pain relief following repetitive transcranial magnetic stimulation of the motor cortex. *Neurophysiol Clin*, **31**, 247-252.

Leijon, G., Boivie, J. & Johansson, I. (1989) Central post-stroke pain--neurological symptoms and pain characteristics. *Pain*, **36**, 13-25.

Li, X.Y., Ko, H.G., Chen, T., Descalzi, G., Koga, K., Wang, H., Kim, S.S., Shang, Y., Kwak, C., Park, S.W., Shim, J., Lee, K., Collingridge, G.L., Kaang, B.K. & Zhuo, M. (2010) Alleviating neuropathic pain hypersensitivity by inhibiting PKMzeta in the anterior cingulate cortex. *Science*, **330**, 1400-1404.

Liu, E.H., Wong, H.K., Chia, C.P., Lim, H.J., Chen, Z.Y. & Lee, T.L. (2005) Effects of isoflurane and propofol on cortical somatosensory evoked potentials during comparable depth of anaesthesia as guided by bispectral index. *Br J Anaesth*, **94**, 193-197.

Liu, J.V., Hirano, Y., Nascimento, G.C., Stefanovic, B., Leopold, D.A. & Silva, A.C. (2013) fMRI in the awake marmoset: somatosensory-evoked responses,

functional connectivity, and comparison with propofol anesthesia. *Neuroimage*, **78**, 186-195.

MacGowan, D.J., Janal, M.N., Clark, W.C., Wharton, R.N., Lazar, R.M., Sacco, R.L. & Mohr, J.P. (1997) Central poststroke pain and Wallenberg's lateral medullary infarction: frequency, character, and determinants in 63 patients. *Neurology*, **49**, 120-125.

Mack, W.J., Komotar, R.J., Mocco, J., Coon, A.L., Hoh, D.J., King, R.G., Ducruet, A.F., Ransom, E.R., Oppermann, M., DeLaPaz, R. & Connolly, E.S., Jr. (2003) Serial magnetic resonance imaging in experimental primate stroke: validation of MRI for pre-clinical cerebroprotective trials. *Neurol Res*, **25**, 846-852.

Mayhew, T.M. (1992) A review of recent advances in stereology for quantifying neural structure. *J Neurocytol*, **21**, 313-328.

McGlone, F. & Reilly, D. (2010) The cutaneous sensory system. *Neurosci Biobehav Rev*, **34**, 148-159.

Migita, K., Uozumi, T., Arita, K. & Monden, S. (1995) Transcranial magnetic coil stimulation of motor cortex in patients with central pain. *Neurosurgery*, **36**, 1037-1039; discussion 1039-1040.

Miyoshi, K., Obata, K., Kondo, T., Okamura, H. & Noguchi, K. (2008) Interleukin-18-mediated microglia/astrocyte interaction in the spinal cord enhances neuropathic pain processing after nerve injury. *J Neurosci*, **28**, 12775-12787.

Moisset, X. & Bouhassira, D. (2007) Brain imaging of neuropathic pain. *Neuroimage*, **37 Suppl 1**, S80-88.

Monif, M., Burnstock, G. & Williams, D.A. (2010) Microglia: proliferation and activation driven by the P2X7 receptor. *Int J Biochem Cell Biol*, **42**, 1753-1756.

Montes, C., Magnin, M., Maarrawi, J., Frot, M., Convers, P., Mauguiere, F. & Garcia-Larrea, L. (2005) Thalamic thermo-algesic transmission: ventral posterior (VP) complex versus VMpo in the light of a thalamic infarct with central pain. *Pain*,

113, 223-232.

Morgado, C., Pereira-Terra, P., Cruz, C.D. & Tavares, I. (2011) Minocycline completely reverses mechanical hyperalgesia in diabetic rats through microglia-induced changes in the expression of the potassium chloride co-transporter 2 (KCC2) at the spinal cord. *Diabetes Obes Metab*, **13**, 150-159.

Mracsko, E. & Veltkamp, R. (2014) Neuroinflammation after intracerebral hemorrhage. *Front Cell Neurosci*, **8**, 388.

Murata, Y., Higo, N., Hayashi, T., Nishimura, Y., Sugiyama, Y., Oishi, T., Tsukada, H., Isa, T. & Onoe, H. (2015) Temporal plasticity involved in recovery from manual dexterity deficit after motor cortex lesion in macaque monkeys. *J Neurosci*, **35**, 84-95.

Murata, Y., Higo, N., Oishi, T., Yamashita, A., Matsuda, K., Hayashi, M. & Yamane, S. (2008) Effects of motor training on the recovery of manual dexterity after primary motor cortex lesion in macaque monkeys. *J Neurophysiol*, **99**, 773-786.

Nagamoto-Combs, K., McNeal, D.W., Morecraft, R.J. & Combs, C.K. (2007) Prolonged microgliosis in the rhesus monkey central nervous system after traumatic brain injury. *J Neurotrauma*, **24**, 1719-1742.

Nagasaka, K., Yamanaka, K., Ogawa, S., Takamatsu, H. & Higo, N. (2017) Brain activity changes in a macaque model of oxaliplatin-induced neuropathic cold hypersensitivity. *Sci Rep*, **7**, 4305.

Nudo, R.J., Wise, B.M., SiFuentes, F. & Milliken, G.W. (1996) Neural substrates for the effects of rehabilitative training on motor recovery after ischemic infarct. *Science (New York, N.Y*, **272**, 1791-1794.

Ongur, D. & Price, J.L. (2000) The organization of networks within the orbital and medial prefrontal cortex of rats, monkeys and humans. *Cereb Cortex*, **10**, 206-219.

Owen, A.M., Evans, A.C. & Petrides, M. (1996) Evidence for a two-stage model of spatial working memory processing within the lateral frontal cortex: a positron emission

tomography study. *Cereb Cortex*, **6**, 31-38.

Percie du Sert, N. & Rice, A.S. (2014) Improving the translation of analgesic drugs to the clinic: animal models of neuropathic pain. *Br J Pharmacol*, **171**, 2951-2963.

Petrides, M. (2000) Dissociable roles of mid-dorsolateral prefrontal and anterior inferotemporal cortex in visual working memory. *J Neurosci*, **20**, 7496-7503.

Petrides, M., Tomaiuolo, F., Yeterian, E.H. & Pandya, D.N. (2012) The prefrontal cortex: comparative architectonic organization in the human and the macaque monkey brains. *Cortex*, **48**, 46-57.

Phillips, M.L., Ladouceur, C.D. & Drevets, W.C. (2008) A neural model of voluntary and automatic emotion regulation: implications for understanding the pathophysiology and neurodevelopment of bipolar disorder. *Mol Psychiatry*, **13**, 829, 833-857.

Ploner, M., Freund, H.J. & Schnitzler, A. (1999) Pain affect without pain sensation in a patient with a postcentral lesion. *Pain*, **81**, 211-214.

Qiu, S., Zhang, M., Liu, Y., Guo, Y., Zhao, H., Song, Q., Zhao, M., Huganir, R.L., Luo, J., Xu, H. & Zhuo, M. (2014) GluA1 phosphorylation contributes to postsynaptic amplification of neuropathic pain in the insular cortex. *J Neurosci*, **34**, 13505-13515.

Raivich, G. (2005) Like cops on the beat: the active role of resting microglia. *Trends Neurosci*, **28**, 571-573.

Rohlfing, T., Kroenke, C.D., Sullivan, E.V., Dubach, M.F., Bowden, D.M., Grant, K.A. & Pfefferbaum, A. (2012) The INIA19 Template and NeuroMaps Atlas for Primate Brain Image Parcellation and Spatial Normalization. *Front Neuroinform*, **6**, 27.

Rosenberg, G.A., Mun-Bryce, S., Wesley, M. & Kornfeld, M. (1990) Collagenase-induced intracerebral hemorrhage in rats. *Stroke*, **21**, 801-807.

Saper, C.B. (1982) Convergence of autonomic and limbic connections in the insular cortex of the rat. *J Comp Neurol*, **210**, 163-173.

Scanley, B.E., Kennan, R.P., Cannan, S., Skudlarski, P., Innis, R.B. & Gore, J.C. (1997) Functional magnetic resonance imaging of median nerve stimulation in rats at 2.0 T. *Magn Reson Med*, **37**, 969-972.

Schmahmann, J.D. & Pandya, D.N. (2006) Fiber pathways of the brain. Oxford University Press New York.

Seghier, M.L., Lazeyras, F., Vuilleumier, P., Schnider, A. & Carota, A. (2005) Functional magnetic resonance imaging and diffusion tensor imaging in a case of central poststroke pain. *J Pain*, **6**, 208-212.

Seifert, F. & Maihofner, C. (2009) Central mechanisms of experimental and chronic neuropathic pain: findings from functional imaging studies. *Cell Mol Life Sci*, **66**, 375-390.

Sharim, J. & Pouratian, N. (2016) Anterior Cingulotomy for the Treatment of Chronic Intractable Pain: A Systematic Review. *Pain Physician*, **19**, 537-550.

Shih, H.C., Kuan, Y.H. & Shyu, B.C. (2017) Targeting brain-derived neurotrophic factor in the medial thalamus for the treatment of central poststroke pain in a rodent model. *Pain*, **158**, 1302-1313.

Sofroniew, M.V. (2009) Molecular dissection of reactive astrogliosis and glial scar formation. *Trends Neurosci*, **32**, 638-647.

Sprenger, T., Seifert, C.L., Valet, M., Andreou, A.P., Foerschler, A., Zimmer, C., Collins, D.L., Goadsby, P.J., Tolle, T.R. & Chakravarty, M.M. (2012) Assessing the risk of central post-stroke pain of thalamic origin by lesion mapping. *Brain*, **135**, 2536-2545.

Steinbacher, D.M. (2001) Propofol: a sedative-hypnotic anesthetic agent for use in ambulatory procedures. *Anesth Prog*, **48**, 66-71.

Strong, K., Mathers, C. & Bonita, R. (2007) Preventing stroke: saving lives around the world. *Lancet Neurol*, **6**, 182-187.

Takami, K., Fujita-Hamabe, W., Harada, S. & Tokuyama, S. (2011) Abeta and Adelta but not C-fibres are involved in stroke related pain and allodynia: an experimental study in mice. *J Pharm Pharmacol*, **63**, 452-456.

Talbot, J.D., Marrett, S., Evans, A.C., Meyer, E., Bushnell, M.C. & Duncan, G.H. (1991) Multiple representations of pain in human cerebral cortex. *Science*, **251**, 1355-1358.

Tamiya, S., Yoshida, Y., Harada, S., Nakamoto, K. & Tokuyama, S. (2013) Establishment of a central post-stroke pain model using global cerebral ischaemic mice. *J Pharm Pharmacol*, **65**, 615-620.

Thibault, K., Lin, W.K., Rancillac, A., Fan, M., Snollaerts, T., Sordoillet, V., Hamon, M., Smith, G.M., Lenkei, Z. & Pezet, S. (2014) BDNF-dependent plasticity induced by peripheral inflammation in the primary sensory and the cingulate cortex triggers cold allodynia and reveals a major role for endogenous BDNF as a tuner of the affective aspect of pain. *J Neurosci*, **34**, 14739-14751.

Tolwani, R.J., Buckmaster, P.S., Varma, S., Cosgaya, J.M., Wu, Y., Suri, C. & Shooter, E.M. (2002) BDNF overexpression increases dendrite complexity in hippocampal dentate gyrus. *Neuroscience*, **114**, 795-805.

Treede, R.D., Kenshalo, D.R., Gracely, R.H. & Jones, A.K. (1999) The cortical representation of pain. *Pain*, **79**, 105-111.

Tsuda, M. (2016) Microglia in the spinal cord and neuropathic pain. *J Diabetes Investig*, **7**, 17-26.

Tsuda, M., Shigemoto-Mogami, Y., Koizumi, S., Mizokoshi, A., Kohsaka, S., Salter, M.W. & Inoue, K. (2003) P2X4 receptors induced in spinal microglia gate tactile allodynia after nerve injury. *Nature*, **424**, 778-783.

Ulmann, L., Hatcher, J.P., Hughes, J.P., Chaumont, S., Green, P.J., Conquet, F., Buell,

G.N., Reeve, A.J., Chessell, I.P. & Rassendren, F. (2008) Up-regulation of P2X4 receptors in spinal microglia after peripheral nerve injury mediates BDNF release and neuropathic pain. *J Neurosci*, **28**, 11263-11268.

Vance, D.E., McNees, P. & Meneses, K. (2009) Technology, cognitive remediation, and nursing: directions for successful cognitive aging. *J Gerontol Nurs*, **35**, 50-56.

Vestergaard, K., Nielsen, J., Andersen, G., Ingeman-Nielsen, M., Arendt-Nielsen, L. & Jensen, T.S. (1995) Sensory abnormalities in consecutive, unselected patients with central post-stroke pain. *Pain*, **61**, 177-186.

Villanueva, L., Desbois, C., Le Bars, D. & Bernard, J.F. (1998) Organization of diencephalic projections from the medullary subnucleus reticularis dorsalis and the adjacent cuneate nucleus: a retrograde and anterograde tracer study in the rat. *J Comp Neurol*, **390**, 133-160.

Wager, T.D., Davidson, M.L., Hughes, B.L., Lindquist, M.A. & Ochsner, K.N. (2008) Prefrontal-subcortical pathways mediating successful emotion regulation. *Neuron*, **59**, 1037-1050.

Wallis, J.D. (2012) Cross-species studies of orbitofrontal cortex and value-based decision-making. *Nat Neurosci*, **15**, 13-19.

Wasserman, J.K. & Koeberle, P.D. (2009) Development and characterization of a hemorrhagic rat model of central post-stroke pain. *Neuroscience*, **161**, 173-183.

West, G.A., Golshani, K.J., Doyle, K.P., Lessov, N.S., Hobbs, T.R., Kohama, S.G., Pike, M.M., Kroenke, C.D., Grafe, M.R., Spector, M.D., Tobar, E.T., Simon, R.P. & Stenzel-Poore, M.P. (2009) A new model of cortical stroke in the rhesus macaque. *J Cereb Blood Flow Metab*, **29**, 1175-1186.

Willoch, F., Schindler, F., Wester, H.J., Empl, M., Straube, A., Schwaiger, M., Conrad, B. & Tolle, T.R. (2004) Central poststroke pain and reduced opioid receptor binding within pain processing circuitries: a [11C]diprenorphine PET study. *Pain*, **108**, 213-220.

Woolf, C.J. & Salter, M.W. (2000) Neuronal plasticity: increasing the gain in pain. *Science*, **288**, 1765-1769.

Yen, C.P., Kung, S.S., Su, Y.F., Lin, W.C., Howng, S.L. & Kwan, A.L. (2005) Stereotactic bilateral anterior cingulotomy for intractable pain. *J Clin Neurosci*, **12**, 886-890.

Yoon, E.J., Kim, Y.K., Shin, H.I., Lee, Y. & Kim, S.E. (2013) Cortical and white matter alterations in patients with neuropathic pain after spinal cord injury. *Brain Res*, **1540**, 64-73.

Yuste, R. & Majewska, A. (2001) On the function of dendritic spines. *Neuroscientist*, **7**, 387-395.

Zhao, B., Shang, G., Chen, J., Geng, X., Ye, X., Xu, G., Wang, J., Zheng, J., Li, H., Akbary, F., Li, S., Lu, J., Ling, F. & Ji, X. (2014) A more consistent intraluminal rhesus monkey model of ischemic stroke. *Neural Regen Res*, **9**, 2087-2094.

Zhao, P., Waxman, S.G. & Hains, B.C. (2007) Modulation of thalamic nociceptive processing after spinal cord injury through remote activation of thalamic microglia by cysteine cysteine chemokine ligand 21. *J Neurosci*, **27**, 8893-8902.

Conclusion

Central post-stroke pain (CPSP) can occur as a result of cerebrovascular accidents in the ventral posterolateral nucleus (VPL) of the thalamus. Here, a macaque model of CPSP based on a focal hemorrhagic lesion in the VPL was developed. Several weeks after induction of hemorrhage, the macaques showed behavioral changes that were interpreted as reflecting the occurrence of both mechanical allodynia and thermal hyperalgesia. Moreover, the macaques showed brain activity changes consistent with pain-related activity in human patients and long-lasting microglial activation that may be characteristic of primate brains. The present macaque model, which reproduces the symptoms of CPSP patients, will contribute not only to understanding the neurological changes underlying CPSP but also to the development of novel therapeutic interventions.

Acknowledgments

I would like to give heartful thanks to Dr. I. Takashima whose comments and suggestions were of inestimable value for my study. I would also like to thank Dr. N. Higo for providing me this precious study and giving me constructive comments. Likewise, I want to thank Drs. M. Shidara, Y. Ichitani, T. Masuda and Y. Kohno for reviewing this thesis and giving me productive comments. I also thank to Dr. K. Matsuda for advice about analysis of MRI data.

I am deeply grateful to Mr. T. Takasu, Ms. A. Muramatsu and Ms. Y. Yoshida for support of this experiment.

Finally, I gratefully appreciate the support and encouragement of my wife, Manae, and my friends.